CHAPTER 9

ION TRANSFER IN AND THROUGH CHARGED MEMBRANES: STRUCTURE, PROPERTIES, AND THEORY

VICTOR V. NIKONENKO, ANDREY B. YAROSLAVTSEV, AND GÉRALD POURCELLY

9.1 INTRODUCTION

The main aim of this chapter is to give a state-of-the-art view on the structure and transport phenomena in charged artificial membranes. This class of materials includes ion exchange, reverse osmosis (RO), and nanofiltration (NF) membranes. All these membranes are largely used in separation processes; the main applications are described in Chapter 20 of this book.

Over the past few years, a remarkable progress in the preparation of membrane materials and in the understanding of their functioning has been made. The significant extent of this progress is due to a relatively novel approach to membranes, regarded as nanomaterials constructed from macromolecules having properties determined by their structure at the nanometer scale. A great number of membranes are obtained by self-assembly strategies allowing the formation of supramolecular structure.[1–4] It is remarkable that the structure and, hence, the properties of biological and artificial membranes have considerable similarities.[1] In both cases, the main elements of the structure are amphiphilic compounds having both hydrophilic and hydrophobic components. The mutual interaction of hydrophobic segments and the interaction of hydrophilic polar groups with aqueous medium result in self-organized stable structures. In particular, nanoscale hydrophilic channels selectively permeable to water and ions are formed within a hydrophobic matrix. In the case of perfluorinated sulfonated ion exchange membranes (IEM) of the Nafion® type

Ionic Interactions in Natural and Synthetic Macromolecules, First Edition. Edited by Alberto Ciferri and Angelo Perico.

YU

(DuPont, Wilmington, DE), the basic structural element has similarities with an inverse micellar morphology. The negative charges of sulfonated groups fixed on the perfluorinated matrix favor cation enrichment within the membrane inner pore solution, so that mainly cations play the role of carriers within the channels transpiercing the membrane body.

In this chapter we try to describe how the structure of charged membranes conditions their properties. Basic approaches to the description of ion and water transfer in such membranes are given. Additionally, we consider surface phenomena accompanying the electric current transfer across IEMs. Concentration polarization and related surface phenomena such as "water splitting" and current-induced convection are described. The mechanisms of these phenomena are analyzed in relation with the properties of a thin surface layer of the membrane. Novel methods of surface modification and the effect of such modification on the overall membrane properties and electrochemical behavior are presented.

9.2 STRUCTURE OF CHARGED MEMBRANES

9.2.1 Biological Membranes: Self-Organizing Systems

A cell membrane is an enclosing film that acts as a selective barrier, within or around the cell.[2,3] Cell membranes control the movement of substances in and out of cells.

According to the fluid mosaic model of Singer and Nicolson,[4] the cell membrane is a complex structure made up of many different components, such as proteins, phospholipids, and cholesterol. The relative amounts of these components vary from membrane to membrane, and the type of lipids can also vary. Amphiphilic phospholipids constitute the major component of the cell membrane. They consist of a phosphate "head" (circles in Fig. 9.1) and a lipid "tail" (lines) that are, respectively, compatible and incompatible with water.

A lipid bilayer is spontaneously formed when the lipid is exposed to water: the hydrophobic "tails" are pointed toward the center of the sheet while the hydrophilic "heads" are exposed to water.

The plane geometry is not the only possible one. In aqueous solution, phospholipids can form two spherical structures as well: the liposome (a closed bilayer), and the micelle (Fig. 9.2).[5,6]

The interior of the bilayer contains almost no water and also excludes nonelectrolyte molecules or salts that dissolve in water but not in oil. The passive transport of water, small noncharged molecules, or ions is facilitated by transmembrane protein channels, which are watery pathways embedded into the lipid bilayer[7,8] and are permanently attached to the membrane. More typically, a cylindrical arrangement of identical or homologous proteins closely packed around a water-filled pore through the plane of the lipid bilayer is observed.[9] Active transport requires additional transmembrane proteins, the transporters, that by complex biochemical reactions and the energy of

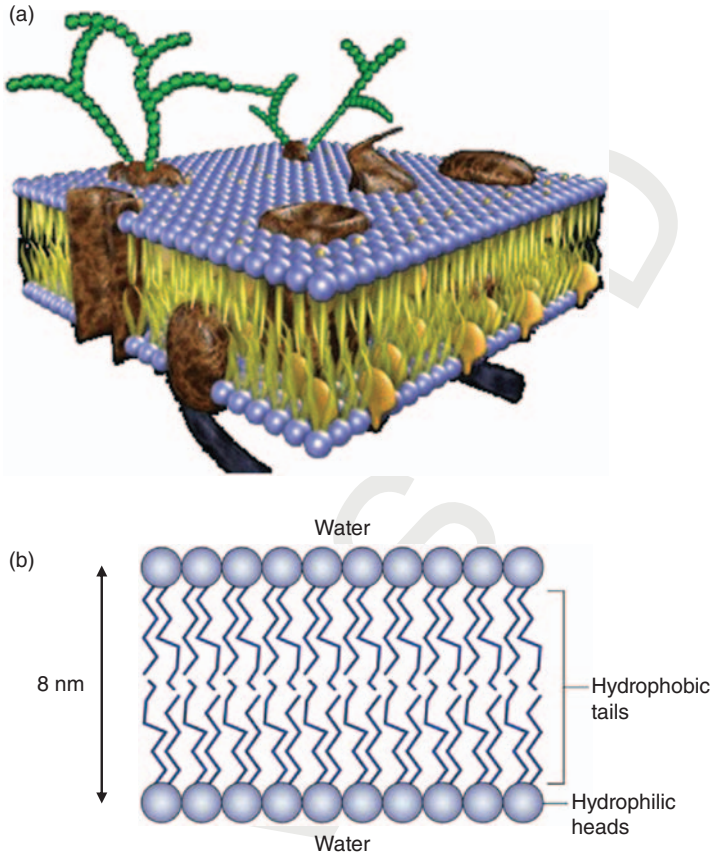

FIGURE 9.1. The structure of a cell membrane (a) and of its main fragment, a phospholipid bilayer (b).

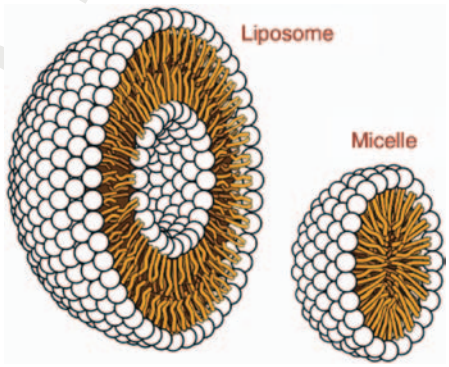

FIGURE 9.2. Spherical structures, which can be formed by phospholipids in solution: the liposome and the micelle. The picture is adapted from Garrett and Grisham.[280]

adenosine triphosphate (ATP) are able to force ions or small molecules through the membrane against their concentration gradient.

This brief description of the cell membranes structure and transport serves to point out similarities and differences between the structure and functionality of biological and synthetic membranes.[1,6] This book contains other chapters treating the interactions and transport in living systems: the protein structure is considered in Chapters 8 and 12, and the iron transport in living cells is described in Chapter 13.

9.2.2 IEMs

Types of Membranes Synthetic IEMs are constructed using flexible polymer chains having aliphatic, aromatic, or perfluorinated residues containing functional groups such as $-COOH$, $-SO_3H$, $-NH_3OH$, and others. Protons or OH^- ions of these groups may be replaced by cations or anions, respectively, present in solutions contacting the membrane. A large number of membrane materials is currently available.[10–12]

The diversity of practical applications of membranes determines a variety of requirements expected from them and, ultimately, promotes the development of a wide range of membrane materials. Generally, IEMs are classified following the charge of the exchanged ions.[13] Thus, the cation exchange membrane can exchange cations associated with the functional groups. For example, in the case of sulfonic acid group, the following reaction occurs:

$$\text{R-SO}_3\text{H} + \text{Na}^+(\text{solution}) \Leftrightarrow \text{R-SO}_3\text{Na} + \text{H}^+(\text{solution}), \tag{9.1}$$

where R is the matrix of membrane. In turn, anion exchange membranes can exchange anions, for example:

$$\text{R-NH}_3\text{OH} + \text{Cl}^-(\text{solution}) \Leftrightarrow \text{R-NH}_3\text{Cl} + \text{OH}^-(\text{solution}). \tag{9.2}$$

Depending upon material structure and the method of preparation, IEMs can generally be divided into two groups: homogeneous and heterogeneous membranes. Homogeneous membranes are obtained by copolymerization of monomers that produces homogeneous material (Fig. 9.3a). Heterogeneous membranes include macroparticles (size from 1 to 50 μm) of different polymer materials; for example, Russian MA-40 (SchekinoAzote, Schekino, Russia) anion exchange membranes include particles of polystyrene–divinylbenzene anion exchange resin and polyethylene (Fig. 9.3b). A more detailed classification, proposed by Molau, includes, in addition to homogeneous and heterogeneous types, interpolymer membranes, microheterogeneous graft and block polymer membranes, and snake-in-the-cage membranes.[14]

A membrane includes one or several layered films. Monopolar membranes have one-film geometry. Bipolar membranes are composed of two layers, a cation and an anion exchange one.[10,11,15–18]

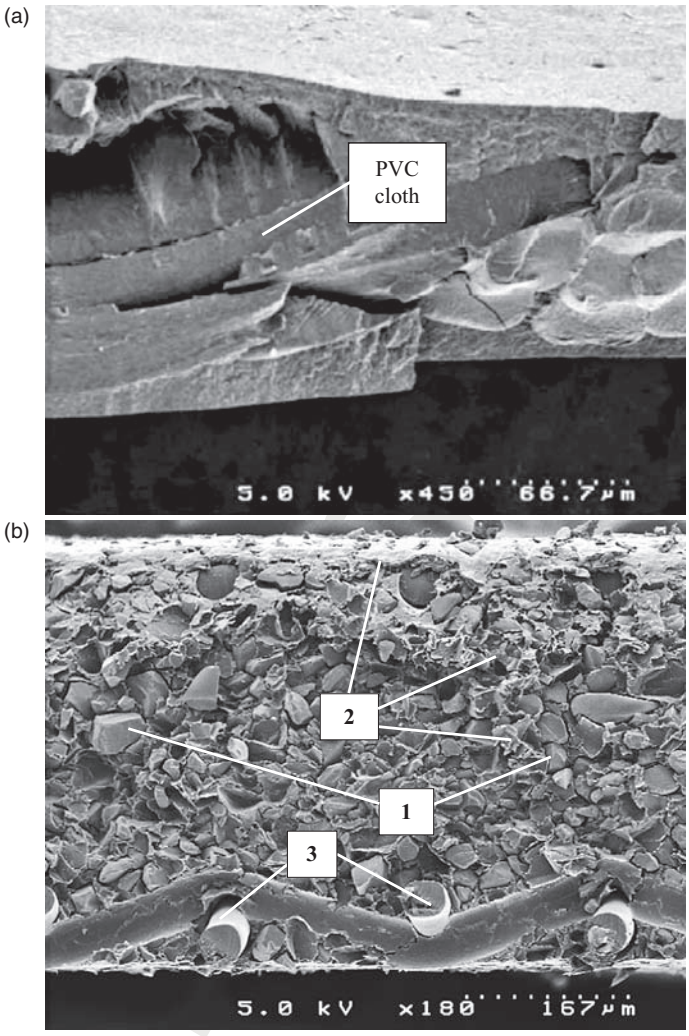

FIGURE 9.3. Electronic microphotographies of IEM. (a) Surface and cross-section of a homogeneous AMX (Tokuyama Soda Co.) anion exchange membrane, a copolymer of styrene, and divinylbenzene[281]; (b) cross-section of a heterogeneous MA-40 anion exchange membrane. 1, ion exchange resin particles; 2, polyethylene; 3, reinforcing cloth.

Supramolecular Interactions and Structuring in Dry State: Phase Separation The main structural feature of IEMs is the hydrophobic backbone of hydrocarbon or perfluorinated chains that antagonizes the hydrophilic character of the functional groups. Together with the flexibility of the polymer chains, this combination leads to self-organization during the formation of membranes.[19,20] With a proper distribution of the hydrophobic and hydrophilic

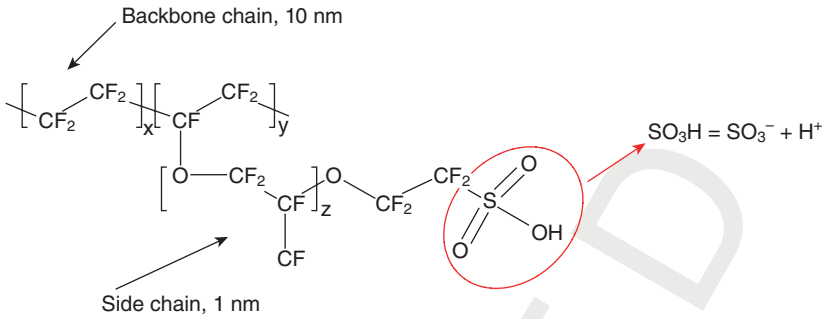

FIGURE 9.4. A perfluorinated sulfonated polymer (supra)molecule. The $-SO_3H$ group is susceptible to dissociate in hydrated state.

components, hydrocarbon or perfluorinated chains act as the matrix of the membrane, while the functional residues are aggregated in small pockets or clusters. The size of these clusters may be in the order of a few nanometers. The hydrophobic component thus contributes to the morphological stability of the membrane, while the hydrophilic domains may provide a system of conducting channels.[20,21]

Perfluorosulfonated acid (PFSA) membranes, in comparison to other types of IEMs, have been studied in more detail due to their applications in *chlor-alkali* production and in fuel cells. Hence, we will focus mainly on this type of membranes, using them as example in order to elucidate their structure–property relation. The chemical structure of the perfluorinated polymer of Nafion membranes is shown in Figure 9.4. The polymer backbone has side chains that carry the sulfonic (or carboxylic) cation exchange groups.[20] The most important feature of the structure in Figure 9.4 is the occurrence of rather long side chains that decouple the motion of the backbone and the charged groups. It is this feature that will facilitate the formation of hydrophilic conducting channels.

Eisenberg[22] and subsequently other authors[20,23–25] suggested that due to dipole–dipole interaction, ion pairs (formed by a fixed ion and a counterion, initially H^+) combine in multiplets able to exclude segments of the hydrophobic backbone (Fig. 9.5). Steric hindrance limits the number of ion pairs in a multiplet. If the number of fixed charges is sufficiently large, and the polymer matrix is sufficiently hydrophobic and elastic, the occurrence of multiplets in larger clusters is favored. The sum of the energies of hydrophobic interactions between backbone segments and of electrostatic attraction between dipoles prevails over the conformational energy of the polymer matrix[25] (Fig. 9.5).

Structure Evolution with Swelling The pores of IEMs containing hydrophilic functional groups are prone to hydration. Even in the dry state, equilibrated with the atmospheric air, a sulfonic acid group in Nafion links two water

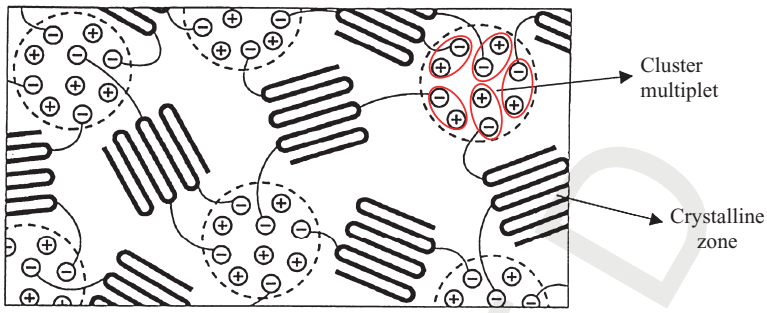

FIGURE 9.5. Structuring of perfluorinated membranes in dry state. Adapted from Shiryaeva and Victorov.[25]

molecules.[21] When an IEM is placed into a water solution, water is adsorbed into the hydrophilic clusters seeking to form ion hydration shells. As a result, the size of clusters increases, and at a certain water content, they form a percolation system.[26–28]

The details of morphology of ion exchange, in particular that of perfluorosulfonic membranes, has been the subject of a great number of publications.[1,20,24,29–32] The main experimental technique applied is small angle scattering with neutrons (SANS) or X-rays (SAXS).[26,29,32,33] The basic model of Nafion morphology, first proposed by Gierke,[23,29] adequately describes its main features and explains the transport properties. The membrane is regarded as a system of hydrated clusters with a diameter of about 4 nm connected by channels with 1 nm in diameter and length. Following Gierke, the side chain charges are located on the periphery of the cluster, which has spherical form in first approximation. This form minimizes the surface energy by reducing the contact of hydrophobic polymer chains with aqueous solution. Thus, the reverse micellar-like structure can be attributed to the membrane: more or less connected spherical aqueous domains are embedded in the hydrophobic polymer matrix (see Fig. 9.6 for low water contents).

The solution filling the inner part of the clusters is charged; it contains mainly counterions produced by the dissociation of functional groups. They neutralize the charge of the side chain charges, forming with them an electrical double layer (EDL). A pore contains a small quantity of co-ions as well, which are ions carrying a charge of the same sign as the fixed ions. The co-ions enter the membrane and are present there, mainly in the pore center zone, under the action of their concentration gradient created by higher concentration of these ions in the outer solution. However, their concentration in the pore solution is generally much lower than that of counterions due to the presence of fixed ions. This effect of ionic disproportion (of uneven ionic distribution) occurring in the solution outside and inside the membrane is called the Donnan effect (see Chapters 9 and 17). Just that causes selective uptake and selective transport (permselectivity) of counterions in IEMs. Figure 9.7 shows

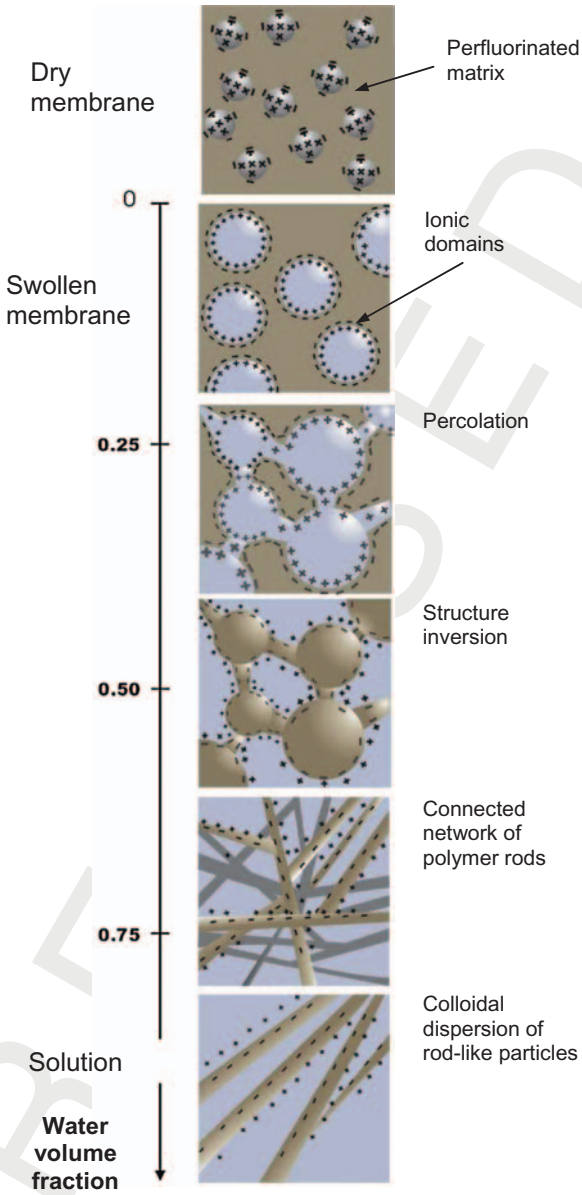

FIGURE 9.6. Evolution of perfluorinated IEM nanostructure with increasing water content. Adapted from Gebel.[26]

schematically the distribution of ions near a pore wall, presented for simplicity as a charged plane.

The structure of EDL at inner interfaces, as well as at outer interfaces, is generally determined by electrostatic interactions and thermal motion. Electrostatic forces result in separation of cations and anions near the charged

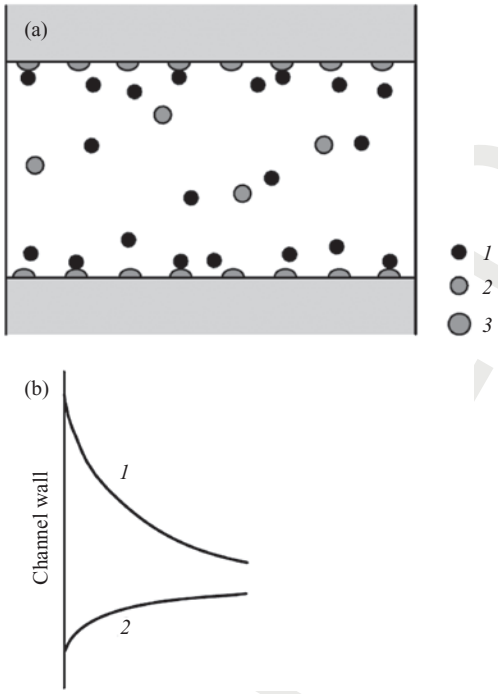

FIGURE 9.7. Counterion (1) and co-ion (2) distribution within a pore near a wall bearing fixed charges (3). The concentration of counterion near the pore wall is essentially higher than that of co-ion. Both concentrations approach that of the external electrolyte with increasing distance from the wall. Adapted from Yaroslavtsev et al.[64]

wall, while the thermal motion tends to equalize the distribution of ions. The distribution of ions within an EDL is described by the Gouy–Chapman theory, taking into account both electrostatic and thermal interaction. This theory gives ion distribution schematically shown in Figure 9.7. Note that the concentration of co-ions in the pore solution decreases with decreasing ratio of the pore radius to the Debye length, the latter characterizing the EDL thickness. Traditionally, when applying this theory, a continuous variation of dielectric permittivity is assumed.[34,35] However, it should be borne in mind that these continuum theories neglect structural inhomogeneity in the vicinity of the inner interface. In particular, Brownian dynamics simulation[36] and other methods[21,34] show that the application of Poisson–Boltzman and Poisson–Nernst–Planck continuum equations leads to an overestimate of the shielding effects (i.e., too high thickness of the diffuse EDL) when the pore radius is less than two Debye lengths.

A number of other investigations of the structure and related properties of Nafion and other perfluorinated membranes were successively reported. Generally, these publications have confirmed the main features of Gierke's model, namely the cluster-channel morphology of these membranes, as well as the characteristic sizes. However, not all the authors agree with the spherical

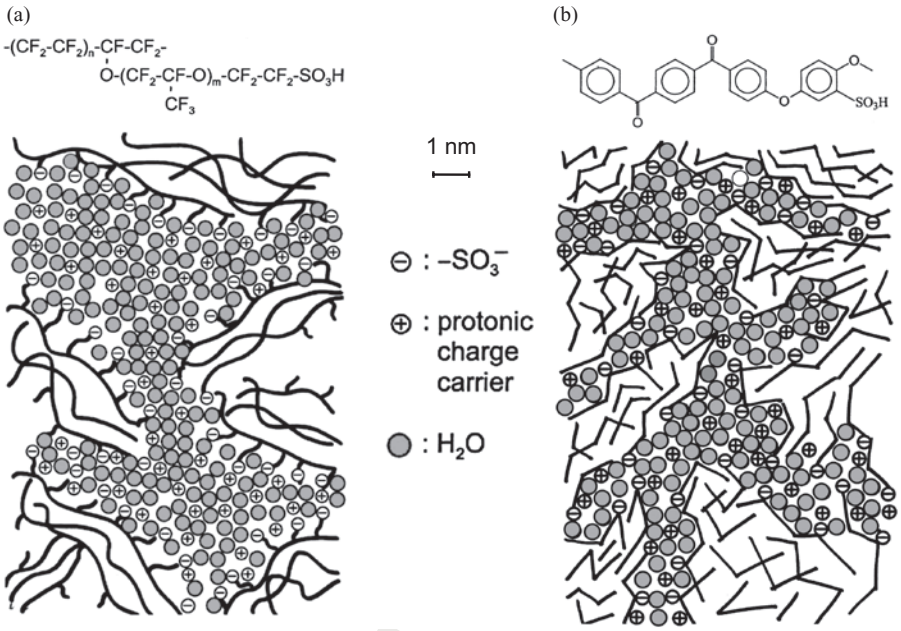

FIGURE 9.8. Two-dimensional structure of a Nafion (a) and a sulfonated polyetherketone (b) membranes on nanometer scale. Adapted from Kreuer.[38]

form of clusters and cylindrical channels argued by Gierke. A review of the papers considering different geometric forms of clusters and channels is made by Rollet et al.[33] In particular, some authors argued for lamellar organization of planar clusters with short connecting channels.[31,37] A rather realistic presentation of two-dimensional structure of Nafion is made by Kreuer[38] (Fig. 9.8a).

At high water contents (which can be attained in commercial perfluorinated membranes at high temperatures in pressure vessels),[26] the membrane structure undergoes essential evolution (Fig. 9.6). Gebel[26] has examined the structure of the swollen PFSA membranes depending on the water content using SAXS and SANS techniques. He has found that at 50% water content, the reverse micellar-like structure transforms into a direct micellar-like one: hydrophobic chains form domains intercalated into the aqueous phase. The side chain charges are located at the polymer/solvent interface and oriented into the aqueous phase. At very high water content, the membrane represents a network of connected polymer rod-like particles: the experimental SANS spectra[26] corresponded to cylindrical particles with 2.5 nm as radius for both the shape and the level of scattered intensity. According to Gebel,[26] the formation of connected cylindrical particles is the best compromise between the minimization of the interfacial energy (which is attained at spherical morphology) and the packing constraints blocking the formation of polymer spheres. Besides, PFSI solutions obtained by using appropriate solvents were studied

by small-angle scattering[39] and magnetic resonance techniques.[40] A colloidal structure formed of polymer rod-like shaped particles was evidenced. The value of the particle radius was found to be between 2 and 2.5 nm, and the length was estimated to be larger than 30 nm.[39]

The size of hydrophilic clusters and their distribution within the membrane depend on such factors as the nature of polymer, concentration of fixed ions, and the degree of polymer cross-linking. Kreuer[38] has carried out a cognitive analysis of the difference in structure and properties of two sulfonic membranes—one with a perfluorinated matrix (Nafion) and another with a polyetherketone one—by applying the SAXS techniques. The polyetherketone backbone is less hydrophobic and less flexible, and the sulfonic acid functional group is less acidic and, therefore, also less polar. As a consequence, the hydrophobic/hydrophilic separation of sulfonated polyetherketones is less pronounced, and the hydrophilic channels are narrower and less connected compared to Nafion (Fig. 9.7). At the same time, the hydrophilic/hydrophobic interface is larger and, therefore, the average separation of neighboring sulfonic acid functional groups is also larger. The water is strongly confined in the narrow channels of the polyetherketone polymers, leading to a significantly lower dielectric constant of the water of hydration (about 20 compared to almost 64 in fully hydrated Nafion).[41] As for the transport properties, the narrower channels in sulfonated polyetherketones reduce the electroosmotic drag and water permeation in comparison to Nafion, while maintaining high proton conductivity, at high water contents.[38]

Role of Side Chains: Swelling in Alcohol Solvents Important information on the side-chain architecture of Nafion was found by Haubold et al.[32] via a SAXS study (Fig. 9.9).

The side chains form a transition region between the aqueous domain and the hydrophobic polymer backbone. The hydration effect of the hydrophilic sulfonic acid groups covalently bounded to the hydrophobic polymer extends within the transition region. Hence, the side chains are partially hydrated. With increasing degree of hydration/solvation, the swelling of the membrane occurs via this region: the side chains unfold in a way that the thickness of the transition region ($s/2$, Fig. 9.9) increases, while that of the purely aqueous region decreases.[32] In aqueous solutions, the $s/2$ value for a Nafion membrane is about 1.7 nm. When methanol (or another alcohol solvent) is present in solution, the membrane swells additionally.[42] For example, in LiCl methanol solution, the thickness of Nafion 117 grows up to 25% and its volume up to 70%.[43] While $s/2$ increases with swelling, the distance between the centers of opposite sulfonic groups (c in Fig. 9.9) decreases.[32] Apparently, when an alcohol is added in an aqueous solution contacting a Nafion membrane, its molecules are initially sorbed by the zones adjoining hydrophobic fragments of the perfluorinated matrix devoid of fixed charges and not available for water. This is in accordance with the lower polarity of alcohol in comparison to water (1.68 and 1.84 Debye for methanol and water, respectively).[13] Hence, there is a

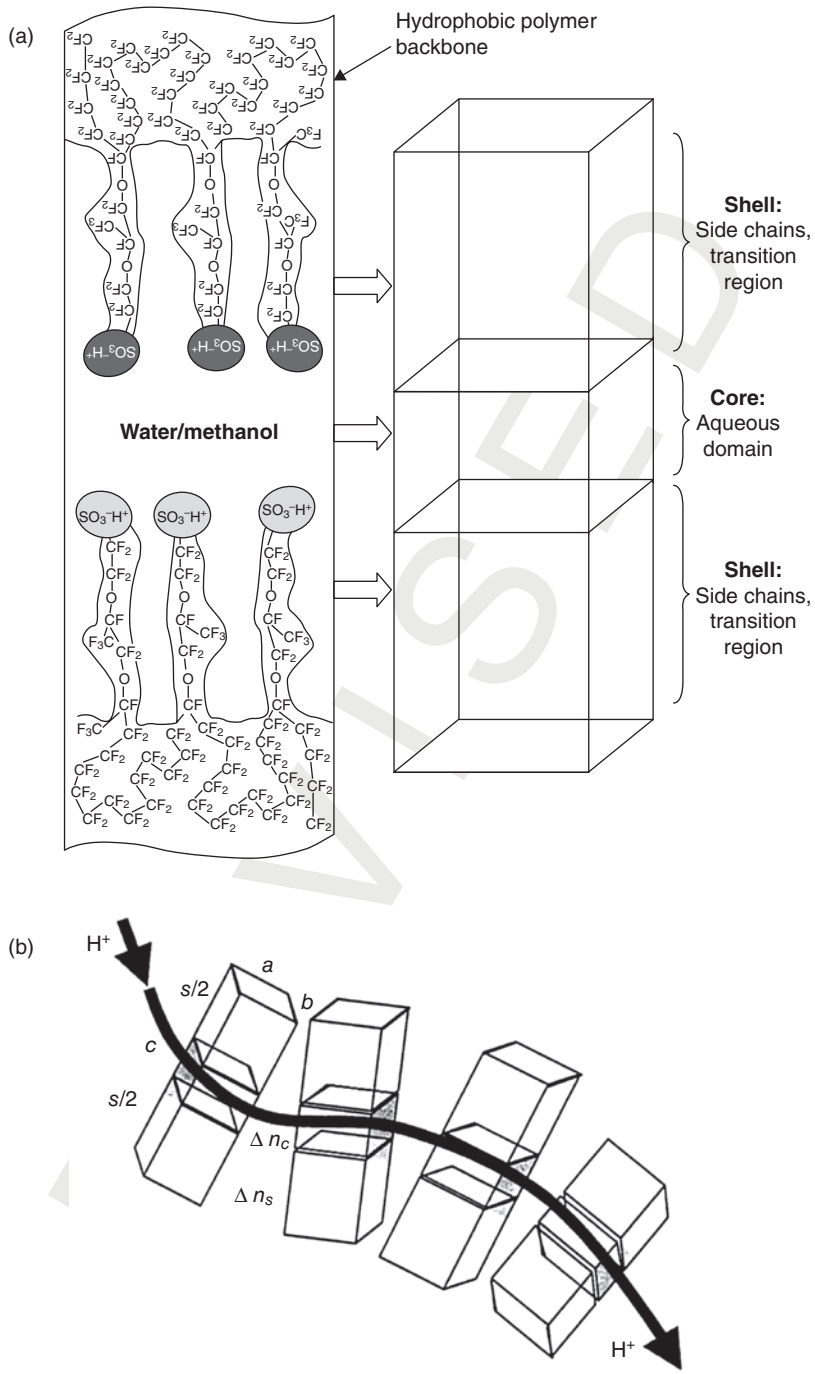

FIGURE 9.9. Schematization of the Nafion structure taking into account the transition region formed by side chains. (a) The main elements of the structure; (b) the passage of a counterion through the membrane. The sense of geometric parameters a, b, c, and $s/2$ is explained in the text. Adapted from Haubold et al.[32]

certain solubility of alcohol in the hydrophobic perfluorinated domains.[44] However, the dielectric constant of water and alcohol is rather different: 81 for water and 32 for methanol. Hence, a noticeable increase in the repulsion between neighboring charged sites should be expected when transferring from water to alcohol solutions. That should lead to an increase of the cross-section of the structure (the product $a \times b$ [Fig. 9.9]),[32] leading to growth of the length of side chains and increase in membrane volume.

The property of side chains to unfold is supported by additional data, for example by electronic structure calculations,[45] showing that the unfolding requires 18 kJ mol^{-1}. Treatment of the Nafion conductivity data led Chaabane et al.[43] to conclude that the space between the charged sites belonging to opposite pore walls (parameter c in the Houbold's model) decreases with increasing methanol content.

Structure of Heterogeneous Membranes Heterogeneous membranes (Fig. 9.3b) are characterized by a more complicated system of pores. Often these membranes are fabricated from ion exchange resin particles (forming ion-conducting phase) and polyethylene (or other bonding agent), strengthening the membrane. The structure of ion exchange resin is similar to that of homogeneous IEMs; it contains micro- and mesopores. Moreover, there are large macropores (cavities, fissures) confined between ion exchange and inert bonding agent.[13] The existence of these two types of pores is evidenced by contact etalon porometry.[46] This method allowed Berezina et al.[47] to obtain pore size distribution for Russian MK-40 (SchekinoAzote) and MA-40 membranes showing two maximums, the first one at about 10 nm and corresponding to micro- and mesopores, and the second one related to macropores having size about 1000 nm. The pores of the first type are located within the ion exchange particles, which are sulfonated (MK-40) or aminated (MA-40) styrene divinylbenzene copolymer. The pores of the second type are the spaces between different particles in a membrane.

Note that sometimes homogeneous membranes contain also inert reinforcing material. For example, Neosepta membranes prepared by the paste method contain a poly(vinylchloride) (PVC) cloth and PVC fine powder constituted of particles much smaller than polyethylene ones in heterogeneous membranes.[48,49] The monomers forming the paste are copolymerized and subsequently sulfonated or aminated to produce IEMs with sulfonic acid or quaternary ammonium groups. Hence, in this case the ion exchange resin produced in the copolymerization presents a continuous phase, which includes PVC particles separated in space and a PVC cloth.

9.3 ION AND WATER TRANSFER IN IEMs

9.3.1 Transfer Mechanisms at Microscale

Ion transport in solutions and organic IEMs is based on two types of transport mechanism at microscale: diffusion in general sense and convection. It is

understood that the movement of ions under the influence of external electric field can also be seen as a diffusion process: migration of an ion in the electric field results from the fact that the frequency of ion jumps in the field direction is higher than in the opposite one.[50–52] Generally, the rate of diffusion processes is determined by the product of the ion mobility and concentration. The first factor is controlled by the nature of the mobile ion and the structure of conducting channels. The ion concentration depends on the charge density of fixed ions and the pore radius. Convective transport is determined by the product of the velocity of the liquid center of mass and the concentration of the given particle.

By analogy with crystals, three diffusion mechanisms may be distinguished in charged membranes: *diffusion by vacancies*, *relay*, *and solvation diffusion*.[50] The first one occurs as a series of jumps from one potential well located near a fixed ion to another one near a neighboring fixed ion, under the condition that the receiving potential well is vacant. In the relay diffusion, the ion can push out a neighboring counterion from its well; the latter passes in interstitial state or pushes out another ion.[50] The solvation mechanism is similar to the ion transport in interstitial space of ionic crystals or in solutions: it is a jump movement from one environment to another.

The height of potential barrier for ion jumps is determined by the energy of electrostatic interactions of hydrated ions, by the chemical interaction of the ion and a fixed group, and by the energy necessary for moving the polymer chains apart to form a channel needed for the passage of ion. The distance between two neighboring wells, λ, should be equal to the distance between two fixed ions and depends on the exchange capacity. For usual ion exchangers, λ is in the range 0.5–1.0 nm[1]; in perfluorosulfonic membranes, this distance within a hydrated cluster is about ~0.8 nm.[1,21]

In the literature considering the transport of protons in PFSA membranes, two mechanisms are discussed[21]: vehicular motion, which is movement of the center of mass of proton in an aqueous environment (solvation diffusion as mentioned above), and structural diffusion or Grotthuss mechanism, which is proton shuttling through hydrogen bonded network.[53] Recently Elliot and Paddison[54] have reported the results of atomistic computational simulations according to which both the vehicular and Grotthuss (relay or shuttling) mechanisms contribute to the mobility of the protons. Zundel and Eigen cations play an important role in charge transport. The $H_5O_2^+$ ions appear to be the dominant charge carriers at relatively low water content, while at higher water contents, $H_9O_4^+$ cations form as solvent-separated ions. The contribution of Grotthuss shuttling increases with increasing water content. Similar results are found in other papers.[55,56]

9.3.2 Heterogeneity on Nanometer Scale and the Role of Dimensions

We have seen in the previous section that ion exchange materials are heterogeneous and there are several scales of heterogeneity. On the nanometer scale,

the homogeneous aqueous media are confined within a hydrophobic phase. This morphology results in relatively narrow transport pores and a very large internal interface. The physicochemical behavior of the conducting domains differs essentially from that of free solutions. First, the internal solution in nanometer pores is charged, as the EDL thickness at the pore walls is of the same order as, if not higher than, the pore radius. The electric current is mainly carried by the ions with the charge of opposite sign vis-à-vis the fixed ions, and that assures the charge permselectivity of IEMs. Second, new transport features, such as electroosmotic drag, occur within the conducting domains.

The transport properties of central parts of the hydrophilic domains differ from that near the internal interface. The very high proton conductivity of hydrated polymers relies on the presence of liquid water as a thermodynamically distinct phase in these domains.[21,45] The water in the center of sufficiently large pores behaves like in free solution.[21,57] The elementary proton transport mechanism there is the same as in the bulk solution: the Grotthuss shuttling is dominant; proton passes from one H_3O^+ (or $H_5O_2^+$ or even larger) complex to a neighboring one.[57] Besides, the dielectric permeability, ε, approaches 81, the value corresponding to free solution (Fig. 9.10). The relative volume of bulk-like water within the pore depends on the water content. According to electronic structure calculations,[21,58] two to three water molecules per sulfonic acid group (n) in perfluorinated membranes are necessary for proton dissociation; when six water molecules are added, separation of the dissociated proton from the sulfonate anion is observed. However, when $n = 6$, all the water within a pore show decreased value of the dielectric permeability (Fig. 9.10). Following Kreuer et al.,[21] only at $n > 14$ it is possible to distinguish the bulk-like water within a pore and to talk about two-phase system there.

The water molecules near the functional groups are structured and largely lose their mobility.[1,21] There is a decrease in polarity and the rate of relaxation, as well as an increase in spatial and orientation order when compared to bulk water; as a result, ε decreases with approaching a functional group (Fig. 9.10). The counterions are concentrated near the functional groups; their mobility there is lower as well; the side chains contribute by increasing the encumbering of the space (Fig. 9.9). At the distance lower than about 0.5 nm from a fixed group, the concentration of counterions decreases due to finite size of hydrated ion. When approaching the pore center, the counterion concentration decreases as well, following the Gouy–Chapman law of ion distribution in EDL (Fig. 9.7).

9.3.3 Functional Properties and Their Relation to the Nanostructure

The main membrane properties, such as permselectivity and conductivity, depend on the ratio of the central and peripheral liquid volumes within the pores. Too high volume of the central part, which occurs in large pores, leads to loss in permselectivity: with increasing pore radius, the co-ion and counterion concentrations become closer, hence, the contribution of co-ions to the

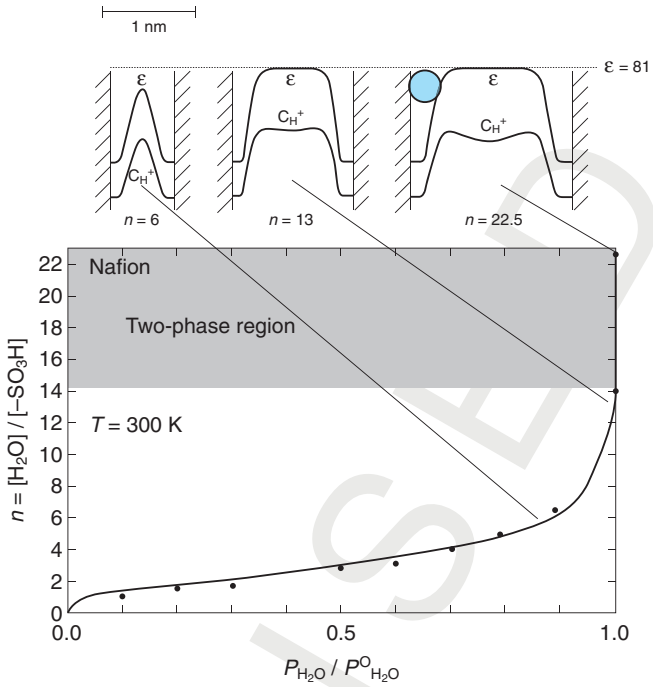

FIGURE 9.10. Hydration isotherm (water content, n, as a function of relative water vapor pressure) for Nafion 117,[162] and the distribution of the dielectric constant[58] and protonic charge carrier concentration across the hydrated hydrophilic pores for three different values of n (top). A hydrated counterion is shown near the pore wall. Adapted from Kreuer et al.[21] T, temperature.

charge transfer increases. The decrease in the amount and the radius of pores results in decreasing conductivity. The membrane morphology can be controlled by changing polymer nature[38] and the concentration of functional groups. In particular, an increase in the length of backbone and side chains leads to increasing the hydrophobic constituent of the membrane and reducing the number and the size of hydrophilic pores.

When the water content increases, the membrane conductivity increases.[26,59] There are several reasons for this. First, the increase in water content enhances percolation between the clusters (see Fig. 9.6), which gives rise to an exponential increase in conductivity according to the common percolation model.[60] Second, when the space available for ion transfer enlarges while the hydrophobic domains remain the same, the average concentration (per unit volume of membrane) and the mobility of ions in the membrane increase.

Note also that the picture of membrane morphology presented above is averaged in time. There is a rapid exchange of molecules between the bulk and interface regions within a pore.[61] Moreover, the pore is not a stiff forma-

tion. Its morphology varies with time within certain limits and has a flickering character.[1]

9.3.4 Irreversible Thermodynamics Approach to Transport Description

There are a number of different approaches to describe ion and water transport in membranes. Some books[52,62,63] and reviews[35,64–66] are dedicated to this subject. Phenomenological approach resulting from the irreversible thermodynamics provides a relatively simple mathematical description, which is however not directly linked to the membrane structure. The structure–properties relations can be described within other approaches, which take into account knowledge on membrane structure, consider the membrane as a multiphase system, and take into account or not the nonuniform distribution of concentrations and electric potential within one phase. In this section, we will consider the principals of mathematical description following these both general axes.

The Onsager Phenomenological Equations The strength and weakness of the description of solute and solvent transfer through the membranes within the framework of irreversible thermodynamics is that no information about the membrane structure and transport mechanism is needed. This approach gives general relations between fluxes and driving forces verified for any type of membrane. The individuality of a given membrane is described through a number of phenomenological coefficients characterizing the system. These coefficients cannot be found within irreversible thermodynamics. Often, their experimental evaluation is sufficient for some engineering purposes. Otherwise, the transport equations given by irreversible thermodynamics should be completed with other equations/boundary conditions, which take into account the details of membrane structure.

At equilibrium, electrochemical potential, μ_i, of any mobile species i (a solvent, an ion, or a molecule) is the same everywhere in the membrane (which can generally have a multiphase structure). If nonzero gradients $d\mu_i / dx$ (for the sake of simplicity we consider one-dimensional [1D] transfer normal to the membrane surface) are present, fluxes of different species appear. When the system is not too far from equilibrium, linear relations between all the fluxes and all the forces can be written as[63,67,68]:

$$J_i = -\sum_j L_{ij} d\mu_j / dx, \tag{9.3}$$

where phenomenological coefficients L_{ij} reflect the effect of thermodynamic force $F_j = -d\mu_i / dx$ on the flux density of species i, J_i. Besides material properties, L_{ij} can depend on the temperature, pressure, and concentrations, but not on fluxes and forces.

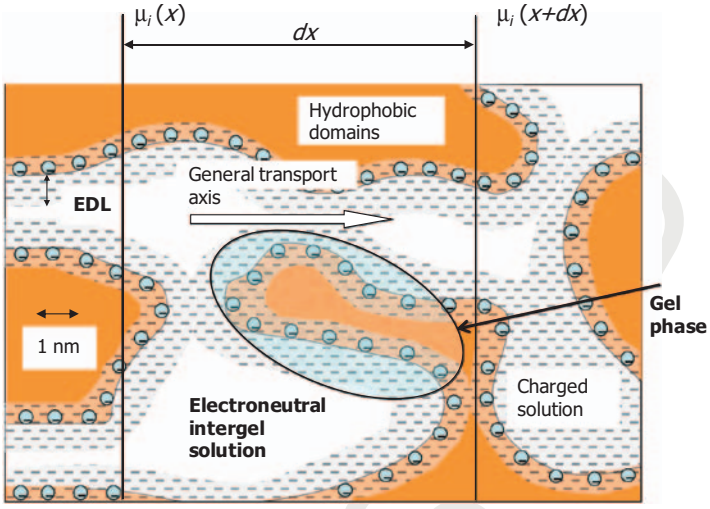

FIGURE 9.11. Schematic presentation of IEM structure including its main elements, in particular fixed ions (shown as circles with –) and electric double layer at the internal interfaces. Gel phase includes fixed ions with polymer matrix and EDL balancing the charge of fixed ions. Adapted from Larchet et al.[150]

To make more physics in the sense of Equation 9.3, note that there is no net transfer in the direction parallel to the membrane surface, and, as a consequence, the electrochemical potential $\mu_i(x)$ is the same at each point belonging to the plane drawn in this direction independently of the phase through which the plane passes (Fig. 9.11). dx in Equation 9.3 may be interpreted as a distance between two planes normal to the transport axis: the first one corresponds to electrochemical potential value $\mu_i(x)$, the second one to $\mu_i(x + dx)$.[52,69,70] dx should be much smaller than the membrane thickness d (to justify the use of differential equation), but noticeably higher than the characteristic size of a phase element, in order that the slice between x and $x + dx$ can serve as a "representative" membrane volume possessing all the structure features. Thus, L_{ij} depends on the properties of all phases present within this slice and varies continuously with x.

Equation 9.3 shows that J_i depends not only on the force applied to species i, F_i, but on the forces applied to other species. The mechanisms of interaction between fluxes of different species (when, e.g., ionic fluxes produced by an electric force give rise to water flow, electroosmosis) are ignored in irreversible thermodynamics.

It is convenient to present L_{ij} coefficients as functions of the concentration of "virtual" electroneutral solution, which is thought to be in local equilibrium with a small volume/thin slice of membrane. The virtual solution was first introduced by Kedem and Katchalsky[71]; it may actually be present in the central part of large pores (if the pore radius is higher than the Debye length) (Fig. 9.11)

or considered as a hypothetical solution (if the double layers at opposite walls of the pores are overlapped). As there is usually local equilibrium at external membrane interfaces, the virtual solution at these interfaces is identical to the solution contacting the corresponding side of the membrane.

The generalized electrochemical potential μ_i in Equation 9.3 can be expressed as a function of concentration c_i (or activity a_i) of species i, electrical potential φ, and pressure p in the virtual solution:

$$\mu_i = \mu_i^0 + RT \ln a_i + z_i F\varphi + \bar{V}_i p, \tag{9.4}$$

where z_i is the charge and $\bar{V}_i$ the partial molar volume of species i; and R, T, and F are the gas constant, the temperature, and the Faraday constant, respectively.

The choice of fluxes (J_i) and conjugated thermodynamic forces (F_i) in transport equations may be different, but not arbitrary: with the right choice of J_i and F_i, the sum of products J_iF_i should give the dissipation function.[63,67] Transport coefficients depend on the choice of fluxes and forces. In the case of the use of Onsager's form, Equation 9.3, coefficients L_{ij} were found experimentally by Narebska et al.[72] for the Nafion 120/NaCl membrane system as functions of NaCl solution concentration. In other forms, with other set of the forces and fluxes, these coefficients are also reported in Spiegler and Kedem[73] and Auclair et al.[74]

Along with Onsager's Equation 9.3, other equations (Stefan–Maxwell, Spiegler, Kedem–Katchalsky, and others)[52,75–78] are used; their review is given in Zabolotsky and Nikonenko[52] and Konturri et al.[63] These systems differ by the choice of fluxes and forces, and consequently, by the transport coefficients; each of them has certain advantages and disadvantages. Generally speaking, they are mathematically equivalent[52] in the sense that it is possible to pass from one system to another by a simple transformation of variables.

The famous Onsager's reciprocal theorem:

$$L_{ij} = L_{ji}, \tag{9.5}$$

allows one to reduce the number of independent phenomenological coefficients. In the case of three different species (a counterion, a co-ion, and a solvent present in a membrane), the number of independent coefficients is equal to 6.

The Kedem–Katchalsky Equations Perhaps it is the system of Kedem–Katchalsky equations[75] that is of the greatest interest for the practical description of transfer through membranes. In differential form, these equations are written as[74]:

$$J_v = -L_p\left(\frac{dp}{dx} - \sigma RTc_s\nu\frac{d\ln a_\pm}{dx}\right) + \beta i = -L_p\left(\frac{dp}{dx} - \sigma\frac{d\pi}{dx}\right) + \beta i, \tag{9.6}$$

$$J_i = -P\frac{dc_i}{dx} + \frac{it_i}{z_i F} - c_i L_p(1-\sigma)\frac{dp}{dx}, \tag{9.7}$$

$$\frac{d\varphi}{dx} = -\frac{i}{\kappa} - \frac{RT}{F}\left(\frac{t_+}{z_+}\cdot\frac{d\ln a_+}{dx} + \frac{t_-}{z_-}\cdot\frac{d\ln a_-}{dx} - \beta c_s \nu F\frac{d\ln a_\pm}{dx}\right) - \beta\frac{dp}{dx}, \tag{9.8}$$

where J_v, J_i, and i are the thermodynamic fluxes (the densities of volume and solute species i fluxes, and the current density, respectively); c_i and c_s are the molar concentration of ion i and that of the salt in the virtual solution of the membrane; π и p are the osmotic and hydrostatic pressures, and φ is the electric potential in the virtual solution, respectively; z_i is the charge number of ion i; $\nu = \nu_+ + \nu_-$ is the stoichiometric number; subscripts $_+$ and $_-$ relate to cation and anion, respectively; and d is the membrane thickness. The form of Equations 9.6–9.8 is so that they are applicable to a cation or an anion exchange membrane. However, let us keep in mind a cation exchange membrane with negatively charged fixed ions; hence, cations will be counterions, and anions, co-ions.

Three thermodynamic forces are considered: mechanical (dp/dx), electric ($d\varphi/dx$), and chemical. The latter is expressed through the gradient of concentration or that of osmotic pressure, which are linked between them[52,75]:

$$\nabla\pi = RTc_s\nu\nabla\ln a_\pm, \tag{9.9}$$

where $a_\pm$ is the mean ionic activity of the electrolyte. Note that the gradient of osmotic pressure can be also expressed through the gradient of water (solvent) activity (a_w)[13]:

$$\nabla\pi = -\frac{RT}{\bar{V}_w}\nabla\ln a_w. \tag{9.10}$$

The equivalence of Equations 9.9 and 9.10 follows from the Gibbs–Duhem equation:

$$c_w\nabla\mu_w + c_s\nabla\mu_s = \nabla p, \tag{9.11}$$

and assumption $c_w\bar{V}_w \approx 1$. It can be verified by substituting Equations 9.12 and 9.13 for water and electrolyte chemical potentials into Equation 9.11:

$$\nabla\mu_w = RT\nabla\ln a_w + \bar{V}_w\nabla p, \tag{9.12}$$

$$\nabla\mu_s = \nu_+\nabla\mu_+ + \nu_-\nabla\mu_- = \nu RT\nabla\ln a_\pm + \bar{V}_s\nabla p. \tag{9.13}$$

Here, $\bar{V}_s$ and $\bar{V}_w$ are the partial molar volume of the solvent and electrolyte, respectively.

The well-known van't Hoff's law for a nonelectrolyte solution ($\pi = c_s RT$) is obtained from Equation 9.10 when using the solvent mole fraction, X_w,

as the solvent activity, and applying the following approximations: $\ln X_w = \ln(1 - X_s) \approx -X_s \approx -n_s / n_w$ and $V \approx n_w \bar{V}_w$. Here n_s and n_w are the mole numbers of the solute and the solvent, respectively, and V is the volume of the system.

The main interest of the Kedem–Katchalsky equations is that the transport coefficients in these equations are just those usually used in characterization of membrane transport properties. For this reason these six transport coefficients are called practical: electrical conductivity (κ); diffusion permeability (P); hydraulic permeability (L_p); transport number of the counterion (t_+); electroosmotic permeability (β); and Staverman reflection coefficient (σ). The sense of the latter may be understood from the following limit cases: $\sigma = 1$, if the membrane reflects completely the solute when it transfers with convective flow through the membrane, and $\sigma = 0$, if there is no retention. The physical sense of coefficients κ, P, and L_p coincides with that of coefficients used in linear equations of Ohm, Fick, and Darcy, respectively, generalized by Equations 9.6–9.8. These linear equations follow directly from Equations 9.6–9.8, if only one driving force is kept nonzero (e.g., the Darcy law results from Eq. 9.6 where $\nabla\pi$ and i are set zero). t_+ shows the fraction of electric charge carried by counterion in conditions where gradients of concentration and pressure are zero; and β is the proportionality coefficient between the volume flux and the current, also under zero gradients of concentration and pressure.

Note that a different form of Kedem–Katchalsky equations is applied as well[75]: instead of the pressure gradient, the volume flux is used in Equations 9.7 and 9.8. This slightly changes the sense of coefficients κ, P, and t_+.[52,75]

Equations 9.6–9.8 are on the basis of membrane characterization.[47,72,78–83] Each of the coefficients terms one of the membrane transport properties, which can be measured under conditions when only one driving force is applied. Thus, diffusion permeability P should be measured when $\nabla p = i = 0$; more details about measuring procedure and the passage from the integral permeability found from the experimentally measured diffusion flux to local coefficient P can be found in Berezina et al.,[47] Zabolotsky and Nikonenko,[52] and Auclair et al.[74]

As we have mentioned above, it is possible to pass from the Onsager to the Kedem–Katchalsky equations by mathematical transformation. Hence, the coefficients present in these two sets of equations are linked.[74,84] Here we present the expressions for κ, t_i, and P,[74] which are the most commonly used parameters:

$$\kappa = (z_+^2 L_+ + z_-^2 L_-)F^2, \tag{9.14}$$

$$t_i = \frac{z_i^2 L_i}{z_+^2 L_+ + z_-^2 L_-} = \frac{z_i^2 L_i F^2}{\kappa}, \quad i = +,-, \tag{9.15}$$

$$P = \frac{2RTg}{c}\left[\frac{\kappa t_- t_{+app}}{F^2} + (L_{+-} - m_s M_w L_{-w})\right] \approx \frac{(z_+ L_+ t_- + |z_-| L_- t_+)RT}{c}, \tag{9.16}$$

where:

$$L_+ = L_{++} + (z_- / z_+)L_{+-}, \quad L_- = L_{--} + (z_+ / z_-)L_{+-} \tag{9.17}$$

are the conductance coefficients of the individual ions $_+$ and $_-$, respectively. The frequently used approximation in Equation 9.16 (the right-hand side after sign ≈) is obtained when assuming $L_{+-} - m_s M_w L_{-w} = 0$, $g = 1$, and $t_{+app} = t_+$, where m_s is the molal salt concentration in the membrane and M_w is the water molar mass. Note that the central part of this equation (after sign =) is written for 1:1 electrolyte, while the right-hand side for any single electrolyte, $c = |z_i|c_i$ is the electrolyte concentration in the virtual solution in Eq dm^{-3}. Similar expressions for L_p, β, and σ can be found in Auclair et al.[74]

The experimental determination of Onsager or Kedem–Katchalsky coefficients is laborious and delicate. This work can be facilitated if one restricts oneself with an incomplete set of coefficients: for example, Staverman coefficient σ is rarely used in ion exchange membrane characterization as it is very close to 1. Another possibility is the use of additional relations between the coefficients.[74,78,84] Such a relation can be obtained[74,84] under the condition that the difference between the cross coefficients reflecting the interaction of co-ions with counterions (L_{-+}) and water ($m_s M_w L_{-w}$) is small compared with the diagonal coefficient L_{--}:

$$P = \frac{2RT\kappa t_- t_{+app} g}{F^2 c}, \tag{9.18}$$

where t_{+app} is the apparent transport number of the counterion, $t_{+app} = t_+ - mM_w t_w$, $m = z_+\nu_+ m_s$, and t_w is the water transport number in membrane; g is the activity factor for the virtual solution[74,85]: $g = 1 + d\ln y_\pm / d\ln c$; and $y_\pm$ is the mean molar activity coefficient.

Equation 9.18 is a generalization of the Nernst–Einstein equation (see the next section) for the case where the osmotic and electroosmotic water transfer are implicitly taken into account. This or similar equations were used and verified[74,79] in different conditions. In the case of perfluorinated Nafion 120 and MF-4SK membranes, a deviation from Equation 9.18 was found,[74] which can be interpreted, following Kedem and Perry,[79] as a consequence of relative hydrophobicity of these membranes.

Equation 9.18 and similar relations[78] are successfully used in the characterization of ion exchange membranes.[74,78,80,82,86] Normally, the transport number t_i^* is easier to calculate from Equation 9.18 or a similar relation when knowing the values of κ and P, in comparison with the evaluation from direct measurements of ionic fluxes.[87]

The Nernst–Planck Equation Together with the laws of Ohm, Fick, and Darcy, it is as well possible to deduce the Nernst–Planck equation from the Kedem–Katchalsky equations. However, that is simpler to do starting from the Onsager Equation 9.3.[51,52,88] If the cross-phenomenological coefficients are

neglected in Equation 9.3 and Equation 9.4 is used with p = const, one immediately finds:

$$J_i = -L_i \frac{d\tilde{\mu}_i}{dx} = -L_i \left(\frac{d \ln a_i}{dx} + z_i F \frac{d\varphi}{dx} \right) \tag{9.19}$$

where L_i is the diagonal conductance coefficient.

The gradient of the electrochemical potential can be expressed through the ion activity (a_i) and electrical potential (φ) in any phase constituting the membrane. In some cases, it is more convenient to use the virtual solution because in this case a_i and φ have not jumped at the external boundaries of the membrane (if only the condition of quasi-equilibrium double electric layers at these boundaries holds true, that is verified at underlimiting current densities).[89–91] L_i characterizes the transport properties of a slice located between planes x and $x + dx$.

When applying Equation 9.19 for a homogeneous phase, the diffusion coefficient of individual ion, D_i, is usually used instead of L_i:

$$D_i = \frac{L_i RT}{c_i}, \tag{9.20}$$

where c_i is the ion concentration in the considered phase. Substituting Equation 9.20 into Equation 9.19 yields:

$$J_i = -D_i \left(\frac{dc_i}{dx} + z_i c_i \frac{F}{RT} \frac{d\varphi}{dx} \right), \tag{9.21}$$

where the variation of the activity coefficient with concentration is neglected.[85,88]

Equation 9.21 is known as the Nernst–Planck equation. It shows that the ion transport occurs under the influence of concentration (the first term in the right-hand side) and electric potential (the second term) gradients.

If not considering the electrochemical gradient as a single driving force, there is no reason to think that the proportionality coefficient before the concentration and electric gradients should be the same. Hence, the equation relating the ionic flux with these two forces is often written in the form[88]:

$$J_i = -D_i \frac{dc_i}{dx} + \frac{z_i}{|z_i|} u_i c_i \frac{d\varphi}{dx}, \tag{9.22}$$

using ionic mobility u_i together with the diffusion coefficient.

Equation 9.22 generalizes formally two linear laws: the Fick and the Ohm laws. When comparing Equations 9.21 and 9.22, we obtain the relation:

$$u_i = D_i \frac{|z_i| F}{RT}, \tag{9.23}$$

known as the Nernst–Einstein relation.

As we have seen, neglecting the cross coefficients in the Onsager equations leads automatically to the Nernst–Einstein relation. This relation is implicitly used each time when Equation 9.21 is applied. It is approximately verified in a number of cases. However, there are deviations related to electroosmotic[92] and/or electrophoretic[93] contributions into electrical conductance, as well as to correlation effects in diffusion[50] and some other effects.[94] Taking into account these deviations is rather complicated. Equation 9.18 gives such an example of taking into account the interactions between counterions and water. It is easy to show that when assuming $g = 1$ and $t_{+app} = t_+$, Equation 9.18 written for a homogeneous phase transforms to Equation 9.23. In this case P is replaced by the electrolyte diffusion coefficient presented (for a single symmetric electrolyte) as $D = 2D_+D_-/(D_+ + D_-)$, where D_i is the diffusion coefficient of the ith *ion*; the transport number of the ith ion is also expressed through D_i: $t_i = D_i/(D_+ + D_-)$. As well, when applied to solution, Equation 9.7 is written with D instead of P, c_i and t_i are referred to the solution, and σ is set to zero (as there is no reflection of any species); product $L_p dp/dx$ may be replaced by J_v, according to Equation 9.6.

The Nernst–Planck equation is widely used in the theory of ionic transfer in membrane systems.[52,63] It is notably simpler than the equations of irreversible thermodynamics, but takes into account two main contributions into ionic transport: diffusion and migration. This equation may be also deduced from the microscopic consideration, which allows one to determine the limits of applicability of this equation[51] when treating the transport at nanometer scale.

There are several generalizations of the Nernst–Planck equation, including the Onsager and Kedem–Katchalsky equations described above. To take into account convective flow, the so called extended Nernst–Planck equation[13,88] is used:

$$J_i = -D_i\left(g\frac{dc_i}{dx} + z_i c_i \frac{F}{RT}\frac{d\varphi}{dx}\right) + c_i V, \tag{9.24}$$

where g is the activity factor (defined above) and V is the center of mass velocity of the fluid flow. Often V is taken as the solvent velocity, which is justified in diluted solutions. Besides, g is assumed to be equal to 1 (as in Eq. 9.21), which is true when the gradient of the activity coefficient is neglected. Instead, g can be calculated using different approaches.[82,83] In the case of 1D flow, V is numerically equal to the volume flux density, J_v. V is calculated as proportional to the gradient of hydrostatic pressure and/or electric potential (electroosmosis)[92] (e.g., with help of Eq. 9.6) or found from experimental volume flux through the membrane. When solution near a membrane is considered, Equation 9.24 is written in two-dimensional (2D) form, and the Navier–Stokes equation is used to find $\vec{V}$.

Convective transport is very important in pressure-driven processes,[95,96] in dialysis across biological or imitating membranes.[97] In the case of IEMs, the convective contribution in the overall transport through the membrane,

expressed by the c_iV term, is rather low. However, this transport is important in fuel cells (water management), in electrodialysis (ED) of concentrated solutions, and in some other cases considered in Section 2.6.

9.3.5 Modeling the Structure–Property Relations

There are a number of models specially developed for linking the structure and transport properties of membranes. Generally, they may be divided in two great groups: *heterogeneous models*, which consider a membrane as a disperse multiphase system; and *continuum models*, describing the transfer within one phase. During the last few years, significant progress was achieved in applying molecular dynamics (MD) for modeling macroscopic behavior of ions and water within a membrane pore.[21] In this method, an ensemble of individual particles is considered, and a system of the Newton equations is solved as time evolving. In this section, these approaches will be briefly described, including some results obtained with the help of MD simulations.

Continuum Models

Teorell–Meyer–Sievers (TMS) Model Historically, the first model successfully applied to explain the main properties of charged membranes was that developed independently in 30 years of the last century by Teorell[98] and by Meyer and Sievers.[99] It is often called the TMS model. This model provides the main ideas of mathematical description of membrane transport and makes the basis of a number of more recent and more sophisticated models.

As we mentioned above, the Nernst–Planck equation is easier to be applied in comparison with complete irreversible thermodynamics approach, as it needs only one diffusion coefficient to be known when describing the transport of an ion. The TMS model is based on this equation; it considers a membrane as a single homogeneous phase (charged gel), which is an aqueous solution of matrix polymer chains, fixed, and mobile ions. Together with Nernst–Planck's Equation 9.21, the local electroneutrality assumption in the membrane:

$$z_+\bar{c}_+ + z_-\bar{c}_- = Q, \tag{9.25}$$

(Q is the concentration of fixed ions, the ion exchange capacity) and surrounding solutions:

$$z_+c_+ + z_-c_- = 0, \tag{9.26}$$

as well as the equation expressing current flowing through the individual ionic flux densities:

$$i = (z_+J_+ + z_-J_-)F, \tag{9.27}$$

and Donnan equilibrium at the interfaces (as boundary conditions):

$$\frac{\bar{c}_+^{1/z_+}}{\bar{c}_-^{1/z_-}} = K_D \frac{c_+^{1/z_+}}{c_-^{1/z_-}}, \tag{9.28}$$

are used to obtain a boundary value problem. The bar under a magnitude signifies that it belongs to the membrane phase.

The Donnan equilibrium relation is obtained when assuming the equality of electrochemical potential for each ion species i present in the membrane/solution system:

$$RT \ln a_i + z_i F\varphi = RT \ln \bar{a}_i + z_i F\bar{\varphi}. \tag{9.29}$$

The ion activities implicitly entering into Equation 9.29 are generally functions of the pressure in each phase. Two relations follow from Equation 9.29: one for activities:

$$\bar{a}_+^{1/z_+} / \bar{a}_-^{1/z_-} = a_+^{1/z_+} / a_-^{1/z_-}, \tag{9.30}$$

and the other for the potential difference (pd) between two phases:

$$\Delta\varphi_D = \bar{\varphi} - \varphi = -\frac{RT}{z_+ F} \ln \frac{\bar{a}_+}{a_+} = -\frac{RT}{z_- F} \ln \frac{\bar{a}_-}{a_-}. \tag{9.31}$$

When introducing ionic concentrations (molar) in Equation 9.30 instead of activities ($a_i = c_i y_i$ and $\bar{a}_i = \bar{c}_i \bar{y}_i$), we arrive at Equation 9.28, where the Donnan equilibrium coefficient, K_D, is expressed through the ratio of mean ionic activity coefficients:

$$K_D = (y_\pm / \bar{y}_\pm)^{1/z_+ - 1/z_-}, \tag{9.32}$$

where $y_\pm = \left(y_+^{\nu_+} y_-^{\nu_-}\right)^{1/\nu} = \left(y_+^{1/z_+} y_-^{-1/z_-}\right)^{(1/z_+ - 1/z_-)^{-1}}$; a similar expression can be written for the mean ionic activity coefficient in the membrane, $\bar{y}_\pm$.

It is assumed (the osmotic theory of adsorption)[13] that the activity coefficients take into account osmotic pressure. Often the $\exp(\Delta\pi \bar{V} / RT)$ term ($\Delta\pi$ is the difference in osmotic pressure between the phases, $\bar{V}$ is the electrolyte molar volume) is introduced separately in the expression for K_D,[13,100] though it is believed that its variation is negligible when analyzing the dependence of $\bar{c}_i$ on c_i.

Usually ion exchange materials have a high concentration of fixed ions (high ion exchange capacity), close to 1 M or higher.[13] This results in a strong exclusion of co-ions, so that their concentration is small in comparison with $\bar{Q}$. When using approximations $\bar{c}_- \ll \bar{Q}$ and $\bar{c}_+ \approx \bar{Q}$, we can simplify Equation 9.28. In the case of a symmetrical electrolyte ($z_+ = -z_- = z$) we obtain:

$$\bar{c}_A = \frac{(K_D)^z}{\bar{Q}} c_A^2, \quad \bar{c}_1 = \bar{Q} + \bar{c}_A, \tag{9.33}$$

where subscript $_A$ is used for the co-ion and $_1$ for the counterion.

The Donnan equation, in the form of Equation 9.28 or 9.33, allows the description of selective adsorption of counterions. Together with this property, the TMS models gives a qualitatively adequate description of other fundamental membrane properties: electric conductivity, transport number, and membrane potential.[101] When introducing another counterion species, 2, and applying Equations 9.28 and 9.31 for each pair 1-A and 2-A, it is possible to describe counterion competitive transfer,[52] bionic potential,[13,102] and so on. This model is widely used for biological as well for artificial membranes.

More details about the TMS model can be found in References 13, 62, and 101.

More recent continuum models may be divided into three groups:

1. Models treating the membrane as a single phase (charged gel), where static and kinetic parameters (concentration of fixed charges, diffusion coefficients, etc.) can continuously change along the coordinate without explicit relation to the structure.[103,104] The option of variation in space of the fixed charge concentration is the feature of these models in comparison with the original TMS theory. Generally, they show that heterogeneity in fixed charge distribution leads to increasing permselectivity in comparison to a membrane having homogeneously distributed charges with the same average concentration. The reason is that the permselectivity is controlled by a layer with the higher local concentration of fixed charge; the layers with low fixed charge concentration have minor impact on global membrane behavior.
2. Capillary models,[105–107] more known as "space-charge models,"[30,108–111] which consider ion and water transfer as occurring within a capillary pore with charged walls.
3. Models applying the percolation theory[112] and simulating the ion transfer by flow of a liquid through a system of voids connected by narrow channels.[1]

Space Charge Capillary Models *Capillary models* are based on the knowledge on membrane nanostructure; they provide detailed information on the transport parameters. First, these models were developed for the description of electrokinetic phenomena within microcapillaries with charged walls. Later on they were improved and adopted for transport phenomena in membranes. These models allow the inclusion of effects specific for interfaces: variation of the dielectric constant with the distance from the pore wall,[108] adsorption,[110] ion hydration effects, finite ion sizes,[113] and others.[110] The role of some of these effects in formation of streaming potential,[114] pore conductivity,[107,115] and permselectivity[116] is studied. This type of model has been shown as very useful in describing the transport of ions and fluid in and around nanometer-sized objects.[117] The research field where the object of study is the fluid transfer in such nanostructures was only recently identified as nanofluidics, but it has a rather rich history, in particular, in membrane science.[118] Nanofluidics has

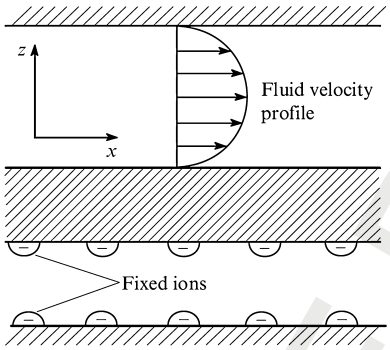

FIGURE 9.12. Schematic representation of the structure of a membrane containing parallel pores with charged walls. The hatched area represents the polymer matrix. Adapted from Zabolotsky and Nikonenko.[52]

experienced considerable growth in recent years, as is confirmed by significant scientific and practical achievements. One hundred nanometers enable the occurrence of phenomena that are impossible at bigger length scales.

Let us consider the main features of space-charge models.

The governing equation describing the ion transport in a pore schematically shown in Figure 9.12 is written in 2D geometry as the extended Nernst–Planck equation with the convective term (Eq. 9.24). The diffusion coefficient is usually assumed to be the same as in free solution. The cross-sectional distribution of local concentration, $\tilde{c}_i$, is described by the Poisson–Boltzman equation.[103] The surface density of the electric charge on the pore wall is σ = 110–440 mC m^{-2}; and the pore radius ranges from 0.5 to 5 nm.[29] The fluid flow (assumed occurring only in axial direction) is described by the Navier–Stokes equation when taking into account the effect of axial pressure gradient and the body force produced by the action of the axial electric potential gradient on the space charge.[105,108]

Calculation of phenomenological coefficients within space-charge models allowed Cwirko and Carbonell[119] and later on other authors[120] to bridge the gap between two different approaches, the irreversible thermodynamics and microscopic model description. Thus, it becomes possible to evaluate macroscopic Onsager's L_{ij} coefficients as functions of membrane nanostructure parameters: the pore radius, charge density of the walls, and others. The authors[119] have compared and calculated experimental (determined by Narebska et al.)[72] L_{ij} coefficients for a Nafion membrane, and found a rather good agreement.

We have mentioned that the use of the continuum Poisson–Boltzman or Nernst–Planck and Poisson equations supposes the ions considered as points; the counterions are permitted to approach too closely the fixed groups that results in overestimation of the shielding effect. Eikerling and Kornyshev et al.[34,113] apply the modified Poisson–Boltzman equation, which takes into

account the size of proton complexes and the real distribution of the charge of the fixed sulfonate groups. In this case, the calculation of the distribution of protons and coulomb energetic barriers is in good agreement with the results of MD simulations.[121] Paul and Paddison[122] have used the Poisson–Boltzman equation in calculations of the hydrated proton self-diffusion coefficient in a Nafion pore through a statistical mechanical model as a function of the distance from the $-SO_3^-$ group. They considered a rather real geometry of cylindrical pores with hydrophobic walls where the sulfonate groups protrude into the pore at some distance (0.4 nm in the calculations) similar to Haubold's model[32] (Fig. 9.9). Following their calculations, the proton mobility is the maximum in the center region of the pore and decreases when approaching the $-SO_3^-$ group; the mobility reaches zero at the distance of about 1 Å to the group. In the vicinity of the $-SO_3^-$ ions the electric field is so strong that the permittivity of water undergoes dielectric saturation, and any positive charge falls are linked to an ion pair that makes negligible its contribution to the ionic current.[122]

Recently Bazant et al.[123,124] have paid attention to the fact that there are steric effects near a wall nonpermeable for ions at high voltages: solvated counterions are crowded there; due to steric repulsion and increased viscosity of the condensed layer, the double-layer capacitance decreases and the electroosmotic mobility saturates, respectively. The former can explain observed high frequency flow reversal in AC electroosmosis.

The *percolation theory*[112] is well adapted for the description of transfer in systems with a developed network of channels, where a part of channels exhibits a good ionic conductivity (such as the clusters in perfluorinated membranes) while the other part shows a low conductivity (the interclusters channels). This theory allows explanation for the dependence of the membrane conductivity on the water content (w) (e.g., in volume percent).[1,59] At low water content, a part of intercluster channels is not conducting; hence, there is no percolation and the clusters present on the left-hand and on the right-hand sides of the membrane are found isolated one from the other. As the water content increases, a more and more increasing number of clusters become connected by channels, thus forming a network penetrating throughout the whole membrane (Fig. 9.6). There is a percolation threshold water content, w_0, corresponding to insulator–conductor transition. At $w < w_0$ the membrane conductivity is nearly zero, while at $w > w_0$ it increases exponentially.[1,59,125]

Multiphase Models Analysis of the structure of charged membranes (Section 9.2) showed that they are porous materials involving in general case micro-, meso-, and macropores. While the definition of these kinds of pores mentions several characteristics (including the length of action of adsorption forces),[126] we will focus only on one parameter: the ratio of the pore radius, r, to the Debye length, λ, characterizing the EDL thickness at the inner pore wall. If $r < \lambda$, we deal with a micropore (normally, $r < 1$ nm); if $r > \lambda$, but r and λ are of the same order of magnitude, we have a mesopore; and if $r \gg \lambda$

($r > 50$ nm), it is a macropore. It is important that in spite of complicated structure of charged membranes, it is possible to distinguish more or less homogeneous regions, which are conventionally called phases.[19] One of these phases comprises electroneutral solution, which fills the central regions of meso- and macropores where the dielectric permittivity and other properties are close to those in free solution[21,45,57] (Fig. 9.10). Homogeneous PFSA membranes such as Nafion contain clusters and channels, which are mesopores and micropores, respectively; there are no macropores; hence, the volume fraction of electroneutral solution is rather small. In the case of heterogeneous membranes, this parameter is several times greater: a relatively large volume of solution is confined in macropores, which are cavities, cracks between ion exchange resin and polyethylene particles. As soon as the first electroneutral phase is distinguished, the remained volume may be referred to the second phase. It is called the "gel phase,"[13,52,70,127] and formed by an ensemble of micropores and the electric double layers in the internal solution of large pores. Besides, this phase includes the fixed charged groups together with the polymer matrix (Fig. 9.11). Sometimes, within the gel phase, the third phase, which is the aggregate of interlaced hydrophobic polymer chains not permeable for ions and solvent, is considered.[70] The third phase may also include (nonconducting) inert binder used to improve mechanical strength, such as polyethylene in heterogeneous membranes.

It is clear that there is no distinct boundary between the intergel electroneutral solution and the EDL that belongs to the gel phase. However this separation represents a useful means, allowing one to simplify the mathematical description. Mafé et al.[128] carried out such a separation within a continuous space charge model when calculating membrane electric conductivity.

The main idea of modeling the transport within a membrane presented as a multiphase system is in attributing to each phase some physicochemical properties, and then to describe the properties characterizing the whole membrane as functions of the single phase properties. Let us consider a macroscopic volume in the form of a layer containing all phases of the membrane (Fig. 9.11). The thickness of this layer, dx, is small as compared to the membrane thickness, and we assume that the phases are in equilibrium with one another. If the matter transfer across this layer is described, in accordance with irreversible thermodynamics, by Equation 9.3 or Equation 9.19 (which is a simplification of the former), the problem is to find the effective transport coefficient L_i, characterizing a layer of thickness dx of the membrane, as a function of coefficients $L_i^{(k)}$, which characterize individual phases k, and the structural and geometric parameters, which describe the shape and mutual position of the phases. This formulation addresses the effective medium approach[129] intensively developed in relation to a great variety of systems and transfer phenomena: electrical conduction,[130] diffusion,[131] heat transfer,[132] optics, and others.[133,134] This approach originated in the work by Maxwell who, in as early as 1873,[135] reported a solution to the problem of conductivity of a system constituting a conductive continuum medium with dispersed spheres

whose specific conductivity differed from that of the medium. A number of researchers, including Rayleigh, Lichtenecker, Bruggeman, Landau and Lifshitz, and others[136–138] contributed to the development of the effective medium approach. The obtained results are often generalized by a hypothesis called "principle of generalized conductivity,"[138] according to which the function relating L_i to $L_i^{(k)}$ is independent of both the nature of applied force and the substance transferred.

As for the application of this approach to ion exchange membranes, several forms of functions relating effective medium conductivity to that of individual phases were proposed. Some of them concern the diffusion,[136,137] the others electrical conductance.[127,136,139,140] Gnusin et al.[70,81,138] have developed a comprehensive model named "microheterogeneous model," which treats conductance coefficients L_i and $L_i^{(k)}$ instead of particular coefficients. This approach allows one to find not only efficient electrical conductivity,[141–144] but diffusion,[145] permselectivity,[146,147] and other[81,148,149] properties starting from one set of membrane parameters.

In the microheterogeneous model, two phases are considered: the gel phase, which is a nanopore medium, globally electroneutral, and including the polymer matrix; and the electroneutral solution filling the inner parts of meso- and macropores, as well as fissures and cavities. The properties of the latter are assumed to be the same as those of the outer equilibrium solution. The relation between the conductance coefficients of individual phases and the effective membrane conductance coefficient, L_i, is expressed in the form[70,138]:

$$L_i = \left[f_1 \left(L_i^g \right)^\alpha + f_2 \left(L_i^s \right)^\alpha \right]^{1/\alpha}, \tag{9.34}$$

where L_i^g refers to the gel phase, and L_i^s to the interstitial electroneutral solution; f_1 and f_2 are the volume fractions of these phases, respectively; α is the structural parameter characterizing the position of the phases in relation to the transport axis: when the phases are disposed in parallel to the transport axis, $\alpha = 1$, in the case of serial disposition $\alpha = -1$, in other cases $-1 < \alpha < 1$.

The gel phase responses perfectly to the assumptions made in the TMS model, hence, this model is used to describe the transport there. Magnitudes L_i^s and L_i^g are expressed by the ionic diffusion coefficients, D_i^s and D_i^g, and the concentrations, c_i^s and c_i^g in the corresponding phases, in accordance with Equation 9.8: $L_i^s = D_i^s c_i / RT$, $L_i^g = D_i^g c_i^g / RT$. Concentrations c_i and c_i^g are linked by the Donnan relations, Equation 9.28 or 9.33, as local equilibrium is assumed between the both phases.

Taking into account that the ions are present in both phases and using Equation 9.33, their concentration in the membrane is written as (for co-ion A)[70]:

$$c_A^* = f_1 \frac{K_D}{Q^g} c_A^2 + f_2 c_A, \tag{9.35}$$

where the first term shows the contribution of the gel phase, and the second that of the interstitial solution; and K_D and Q^g are the Donnan coefficient and the exchange capacity of the gel phase, respectively. In spite of small value of f_2 (typically less then 0.1 in homogeneous membranes and about 0.2 in heterogeneous ones), the electrolyte sorption by the "intergel" phase is dominant, especially in diluted solutions, due to co-ion exclusion from the EDL in micro- and mesopores. For this reason, the amount of electrolyte sorbed by the gel is small, and Equation 9.33, which is an approximation of the Donnan relation presumed to be true for diluting solutions of strong electrolytes, is verified for concentrations up to 1–2 M, for conventional IEMs.

Thus, the membrane equilibrated with a binary solution is characterized by six parameters: two static, K_D and Q^g; two structural, f_1 and α; and two kinetic ones, diffusion coefficients of counterion, D_1^g, and co-ion, D_A^g, in the gel phase. It is assumed that the diffusion coefficients in the interstitial solution, D_i^s, are the same as in free solution. When knowing these parameters, L_i coefficients can be calculated as functions of the interstitial solution concentration, as was explained above. Then the electrical conductivity, κ, the ion transport number, t_i, and the diffusion permeability, P, can be calculated by using Equations 9.14–9.16, giving the links between the coefficients of transport equations written in Onsager's and Kedem–Katchalsky's forms. Equations 9.14–9.16 can be applied at any coordinate in a membrane considering c as the local concentration. Thus, the microheterogeneous model can be incorporated into a number of boundary value problems modeling the ion and solvent transfer in membrane systems.[150,151]

To find the parameters of the microheterogeneous model, some experiments should be made and the data obtained treated. To determine all six parameters, ion exchange capacity, electrolyte uptake, conductivity, and diffusion permeability—all properties as functions of electrolyte concentration—should be found. The algorithm of data treatment is described in Zabolotsky and Nikonenko.[52] However, often only some parameters between the six are of interest. For example, the volume fraction of the gel (or intergel phase) is a quite important characteristic of membrane. This parameter may be relatively easily found from the concentration dependence of membrane conductivity (κ_a) under alternative current. Equation 9.28a allows a simple approximation at $\alpha \to 0$[70]:

$$\kappa_a = \left(\kappa^g\right)^{f_1} \left(\kappa^s\right)^{f_2}. \tag{9.36}$$

Since the gel conductivity, κ^g, only slightly depends on electrolyte concentration (as the co-ion sorption by the gel is very low), the $\ln \kappa_a - \ln \kappa^s$ correlation, according to Equation 9.36, should be linear with f_2 as the slope. Numerical calculations show that near the "isoconductance point" (where $\kappa_a = \kappa^g = \kappa^s$), κ_a is almost independent on α,[70] and in the range of $0.1\ c_{iso} < c < 10\ c_{iso}$ the $\ln \kappa_a - \ln \kappa^s$ dependence may be approximated by a straight line up to $|\alpha| = 0.2$. Taking into account that for most ion exchange membranes α lays in the range

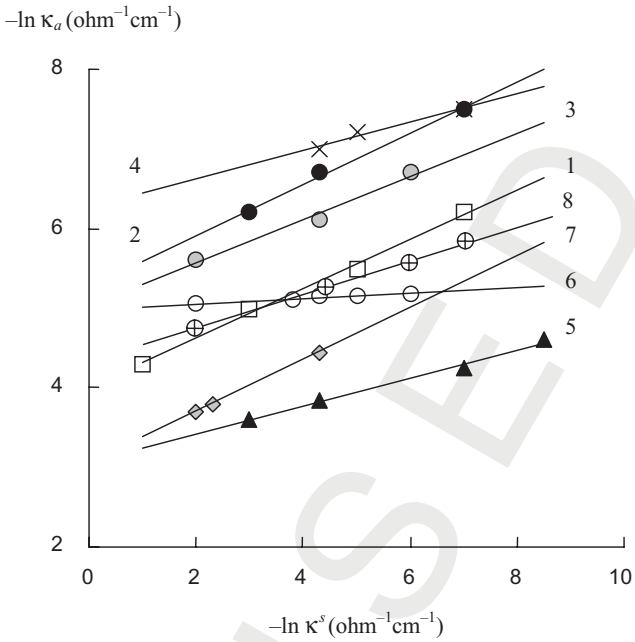

FIGURE 9.13. Specific conductivity of IEMs under AC (κ_a) as a function of solution-specific conductivity (κ^s) in ln–ln coordinates for different membranes. 1, C-60/65 in HCl; 2 and 3, Amberplex C-1 in NaCl and KCl, respectively; 4, Amberplex A-1 in NaCl; 5, AMF C-103 in NaCl; 6, MF-4SK in NaCl; 7, Nepton CR-61 in KCl; 8, MK-40 in NaCl. Adapted from Zabolotsky and Nikonenko.[52]

0.1–0.3, Equation 9.36 may be confidently applied, if the concentration is not too far from the isoconductance point c_{iso}. As Figure 9.13 shows, the slope for the homogeneous membranes (MF-4SK, AMF, CM2) is essentially lower than that for the heterogeneous ones. Thus, f_2 is equal to 0.01 for a perfluorinated MF-4SK, and about 0.2 for heterogeneous MK-40; this quantity reaches 0.45 for a special macroporous membrane.[141]

Zabolotsky and coworkers[141,152] have compared the values of f_2 found from conductivity measurements and applying Equation 9.36, and by using other methods: sorption of electrolyte, standard contact porosimetry,[46] and differential scanning calorimetry (DSC). The close values of f_2 obtained (e.g., for a MK-40 membrane: 0.17 ± 0.02 from conductivity[141]; 0.1 ± 0.02[152] and 0.26 ± 0.02[141] from sorption; 0.23 ± 0.05 from porosimetry[141]; and 0.21 from DSC)[141] testifies that the microheterogeneous model adequately presents the membrane structure and the transport laws.

The facility of use of Equation 9.36 for treatment of experimental conductivity data, which are often available, the possibility to describe other important properties, the diffusion permeability, and the ion transport numbers,

result in the fact that this model has been shown as a quite suitable for ion exchange membrane characterization.[12,47,143,144,147,153–157]

There is interference of the microheterogeneous model with other, more detailed structural models, namely with the Haubold model,[32] built on the basis of SAXS experimental data. From the measurements of electric conductivity of a Nafion 117 membrane in mixed water–methanol LiCl solutions and the treatment of the data with the microheterogeneous model, it was found[43] that the volume fraction of electroneutral interstitial solution (f_2) in the membrane decreases with increasing methanol content in solution (X_{MeOH}), at least at $X_{MeOH} < 60$ vol %. The same result was obtained by evaluating f_2 with the help of the Haubold model and parameters resulted from SAXS measurements. The decrease in f_2 with growing methanol content (and growing overall membrane swelling) is explained by unfolding of side chains during membrane swelling in methanol (see Section 1.2 and Fig. 9.9). The latter results in a decrease in the distance between the sulfonic ions bonding to the opposite walls of the pore.

9.3.6 Water Transport

Thermodynamic Consideration: Total Driving Force While the considered above models deal with the membrane transport of ions as well as water (or other solvent), they are mainly directed at the ion transfer description. In literature, water transfer is given special attention. The understanding of this phenomenon is important for improving dialysis and ED as well as fuel cells. In fuel cells, the so called water management[158–160] is one of the major problems in low-temperature technology as partial dehydration of proton-conducting membrane results in sharp increase of its resistance.[21,42] In ED, high water flux does not allow concentrated brine to be obtained.[10] On the other hand, water transfer contributes greatly in effective work of bipolar membranes.[161]

The mechanisms of water transport in membranes, similarly to the ion transport, include self-diffusion; chemical or Fickian diffusion produced by gradient of water chemical activity; and permeation produced by a hydrostatic pressure gradient, which is convection transfer. The water transport occurring under the action of electric field and caused by the interaction between counterions and water molecules (electroosmotic drug)[21,35] is often considered apart as no external force is applied to water molecules.

Generally, the thermodynamic force applied to water is expressed as the gradient of water chemical potential and includes, in accordance with Equation 9.4, the hydrostatic pressure gradient and the gradient of Napierian logarithm of water activity:

$$\nabla \mu_w = RT \nabla \ln a_w + \bar{V}_w \nabla p, \tag{9.37}$$

where $\bar{V}_w$ is the partial molar volume of water. Note that Equation 9.37 may be applied also to other solvents; thus, the subscript $_w$ denotes any solvent in

general case. As the osmotic swelling pressure (π) inside the membrane is linked with the solvent activity (a_w)[13]:

$$\pi = -\frac{RT}{\bar{V}_w} \ln a_w, \tag{9.38}$$

in any case where a gradient of water chemical potential occurs, a swelling pressure gradient is induced. In particular, when a membrane separates two solutions of different concentration, the water transfer occurs as chemical diffusion and permeation.[21,62]

Substituting Equation 9.38 into Equation 9.37 yields:

$$\nabla \mu_w = \bar{V}_w \nabla (p - \pi). \tag{9.39}$$

This equation enables linking the water chemical potential gradient with $\nabla(p - \pi)$, that is, the difference between the hydrostatic and osmotic pressures, which was called[21] "total pressure" gradient. Thus, the "total pressure" gradient can be considered as a unique driving force of solvent transfer. Due to Equation 9.39, a correlation between the "chemical" (found from chemical diffusion data) and "permeation" (found from solvent permeation experiments) diffusion coefficients can be established.[21] As follows from papers by Kreuer et al.[54,162] and other authors[163,164] reviewed in Kreuer et al.,[21] the "permeation" diffusion coefficient is always greater than the "chemical" one. This result is not expected if the elementary mechanisms of water transport are the same in chemical diffusion and permeation water transfer.[21] The reason of permeation transport "priority" is that in addition to quasi-random walk process there is another transport component. That is, following Kreuer et al.,[21] viscous flow accompanied by a certain "slip" at the interface with the hydrophobic domain. It is known that in macroscopic systems this slip introduced by Navier is negligible.[88] However, it becomes important in micro- and nanometer channels.[165,166] The situation with the correlation between two types of water transport is similar to that occurring when counterion diffusion coefficient found from diffusion measurements is compared with that obtained from conductivity data by applying the Nernst–Einstein relation, Equation 9.23. In this case the second value is often higher mainly because of additional transport mechanism, electroosmosis, generating solvent flow within membrane pore, and facilitating counterion transport in the same direction (convection conductivity).[13,94]

On the basis of Equation 9.39, the water flux density in the membrane may be written as (in 1D geometry):

$$J_w = J_w^o + J_w^{eo} = -A \frac{d(p - \pi)}{dx} + \frac{t_w i}{F}, \tag{9.40}$$

where coefficient A is proportional to the membrane hydraulic permeability and inversely proportional to the water viscosity[167] as it takes place in

classical Darcy's law originally formulated for the hydrostatic pressure gradient only.

Equation 9.40 contains two terms. The first one represents the Darcy law written for the "total pressure" gradient and describing the solvent flux under the action of the external pressure gradient (hydraulic filtration) and the capillary (or swelling) pressure gradient (osmotic flux)[168]; the latter being proportional to $d\pi/dx$. When an electric current of density i is applied, the second term, the electroosmotic flux, proportional to the product of i and the water transport number, t_w, is added.[167] Instead of t_w, often the water drug coefficient is used in Equation 9.40. The latter shows the number of water molecules transported per proton,[169] while t_w is the number of water moles transferred through the membrane with one Faraday of electricity.[62,170]

Note that the term proportional to $d\pi/dx$ may be written also as $-D_w dc_w/dx$ with diffusion coefficient, D_w, and concentration, c_w, of water in the membrane,[171] when taking into account Equation 9.10. In this case, the Fickian mechanism of water transport is emphasized.

The use of the "total pressure" in the Darcy equation is justified by clear correlation between the swelling and the microscopic growth of the clusters in Nafion.[172] The involving of pressure gradient in water transfer phenomenon through an ion exchange membrane is well explicated by a scheme proposed by Meier and Eigenberger[167] (Fig. 9.14). This scheme is in conformity with the membrane structure models reviewed above (Section 9.1), which take their origin from the cluster channel model of Gierke.[23] On the side of high water activity (diluted solution or pure water), the swelling of hydrophilic domains (clusters) produces an increase in their size and an increase in the tension of polymer chains; the elastic matrix of the membrane is more strongly stretched at this side. On the side of low water activity (concentrated solution), the size of clusters and the tension of elastic matrix is lower.

When starting from irreversible thermodynamic approach, one arrives at a similar phenomenological description of the solvent transfer, which is the

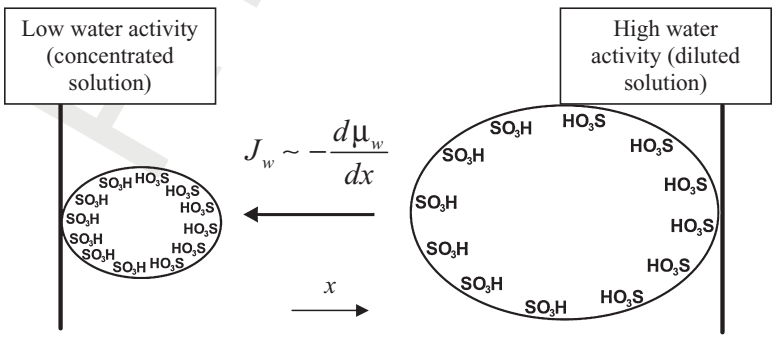

FIGURE 9.14. Scheme of involving pressure gradient in water transfer phenomenon. Adapted from Meier and Eigenberger.[167]

Kedem–Katchalsky equation in the form where the gradient of osmotic pressure enters explicitly as a driving force, Equation 9.6:

$$J_v = -L_p\left(\frac{dp}{dx} - \sigma\frac{d\pi}{dx}\right) + \beta i. \tag{9.41}$$

The difference between Equations 9.40 and 9.41 is in the fact that Equation 9.40 is applied to the transfer of water while Equation 9.41 to that of the volume, $J_v = \bar{V}_w J_w + \bar{V}_s J_s$, where $\bar{V}_s$ and J_s are the partial molar volume and the flux density of the solute, respectively. As a consequence, the reflection coefficient σ appears in Equation 9.41. For better understanding, consider the situation where a membrane separates pure water and a solution. The water flux through the membrane is zero, if, according to Equation 9.40, the difference in hydrostatic and osmotic pressures across the membrane is zero: $\Delta p = \Delta\pi$. However, the volume flux is zero if $\Delta p = \sigma\Delta\pi$, Equation 9.41. In the last case, the water flux is not zero, but the volume transferred by water is compensated by that transferred by the solute in the opposite direction. The water flux becomes zero only if the solute reflection is ideal: $\sigma = 1$.

The importance of involving σ becomes more evident when considering the so-called anomalous osmosis through a membrane.

Anomalous Osmosis The Darcy law under the form of Equation 9.40 as applied to osmotic transfer (when $\nabla p = i = 0$) assumes that the solvent flux is proportional to the difference in osmotic pressures between two solutions separated by the membrane, and the direction of this flux is from the more diluted solution into more concentrated one. However, in several cases the solvent flow deviates from this law. Anomalous osmosis was observed in numerous ion exchange membranes,[106,173,174] including Nafion.[174] In the case of positive anomalous osmosis, the solvent flux is higher than it can be expected from the Darcy law; and in negative anomalous osmosis the situation is presented as inverse: the solvent flux is low and even may be directed from the more concentrated into the more diluted solution.[13,62] The theory of anomalous osmosis was developed by Schlögl[175] and later by Kedem and Katchalsky,[75] and others.[106,176] The reason of anomalous osmosis is that the osmotic pressure is not the only driving force for solvent transfer.[13] The other driving force is the gradient of electric potential induced due to the difference in diffusion mobilities of co- and counterions in membrane pores.[13,62] As follows from the theory of Kedem and Katchalsky,[75] based on the irreversible thermodynamics and frictional forces formalism, the negative anomalous osmosis may be expected in the case where the electrolyte flow across the membrane is elevated (the membrane permeability and electrolyte concentration are high), and the counterion transport number is low; the reflection coefficient σ is then negative. In this case, the co-ions diffuse within a membrane pore faster than the counterions at the beginning that gives rise to an electric field accelerating the flow of counterions. Co- and counterions diffusing from the more

concentrated to the less concentrated solution transport water in the direction, which is opposite to that of the water osmotic flux. If the flux of water transported with ions is higher than the osmotic flux, the overall water flux becomes directed toward the diluted solution. Koter[106] has modeled the osmosis transfer in the framework of a space charge capillary model, and found that the negative osmosis for an anion exchange membrane (AM1) with a HCl solution can be explained if one assumes a relatively low transport number of Cl^- counterion and a high mobility of H^+ co-ion in the membrane.

Ion Transfer by Convection in IEMs The contribution of different terms in Equations 9.40 and 9.41 depends on the membrane and solution under study. As well, the mechanism of ion transfer becomes dependent on the peculiarities of the solvent transfer. Bobreshova et al.[177] and Shel'deshov et al.[178] have evaluated the contribution of the ion convection transport within the pores of heterogeneous membranes when varying the hydrostatic pressure difference, the electrolyte concentration, and the current density. They have applied the extended Nernst–Planck equation, Equation 9.24, taking into account that the convection is caused by both electroosmotic and pressure-driven water transfer. By comparing their simulation with experimental data, the authors[178] have found that the convective transfer through the MA-40 heterogeneous membrane is controlled by an array of mesopores connecting two neighboring macropores. This result is conformed with the hydrodynamic model of fluid flow in biporous media developed by Filippov et al.[134,179] The electroosmotic contribution decreases with increasing electrolyte concentration (due to reduction of the EDL), and at 2 M NaOH the pressure-driven contribution to the convection caused by a small pressure difference in 30 kPa becomes about 10 times higher than the electroosmotic one. Hence, when applying a pressure difference across a membrane together with an electric current, it becomes possible to operate the convection flux. For example, if a sufficiently elevated pressure is applied in the concentration compartments of an ED stack, the solvent is driven out of these compartments, and a more concentrated solution is obtained. This is especially important when using hydrodynamically closed concentration compartments without solution circulation (Fig. 9.15; see also Chapter 19 of this book). Generally, combining electric and pressure gradients across a membrane opens up large possibilities in operating ED separation and concentration.

Water Transfer in an ED Cell Equations 9.40 and 9.41 are applicable to one membrane. In an ED stack (Fig. 9.16a), cation and anion exchange membranes are alternatively arranged to form desalting and concentrating compartments[10–12] (see also Chapter 21). For describing an ED process, at least two membranes making an elementary cell with one desalting and one concentrating compartments should be involved. Zabolotsky et al.[52,180] have developed a model for ion and solvent transfer for an ED cell with a cation and an anion exchange membranes where there is no circulation through the concen-

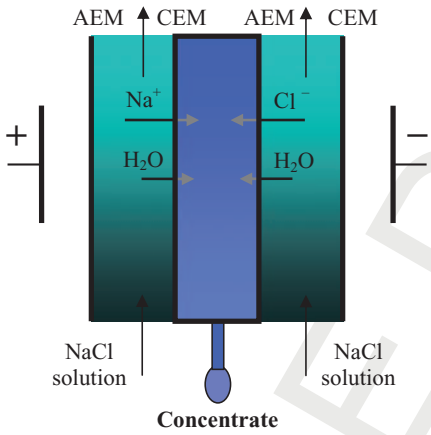

FIGURE 9.15. Scheme of an ED cell involving a concentration compartment with closed entrance for feed solution. AEM, anion exchange membrane; CEM, cation exchange membrane.

tration compartment: the entrance is closed (Fig. 9.15). Water enters this compartment by electroosmosis, mainly within the hydration shell of counterions. The concentrate flows out via a capillary.

The transport equations applied in the model result from integration of the Kedem–Katchalsky equations. The total fluxes of salt (s) and water (w) through both membranes into the concentration compartment are written as follows[52,180]:

$$J_{s\,tot} = -P_s(c_b - c_d) + \eta\frac{i}{F}, \tag{9.42}$$

$$J_{w\,tot}P_w(c_b - c_d) + t_w\frac{i}{F}, \tag{9.43}$$

where $P_s = P_s^a + P_s^c$ and $P_w = P_w^a + P_w^c$ are the electrolyte diffusion and water osmotic permeabilities related to the cell pair, respectively; P_s^a, P_s^c, P_w^a, and P_w^c relate to anion exchange (a) and cation exchange (c) membranes, respectively; $t_w = t_w^a + t_w^c$ is the water transport number per cell pair; $\eta = 1 - t_+^a - t_-^c$ is the current efficiency of electromigration transfer; and c_b and c_d are the electrolyte concentration in concentration (brine) and desalination compartments, respectively.

The brine concentration expressed in mole fractions is found as:

$$N_s = \frac{j_{s\,tot}}{j_{s\,tot} + j_{w\,tot}}. \tag{9.44}$$

The results of calculations of N_s as a function of current density with the use of Equations 9.42–9.44 are in a good agreement with the experiment.[180] The

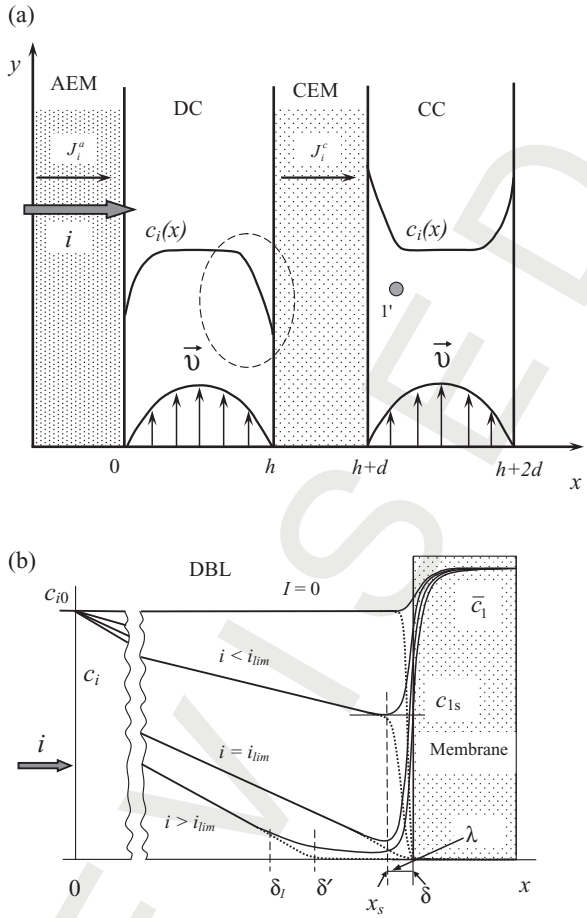

FIGURE 9.16. (a) Scheme of an ED cell with anion exchange (AEM) and cation exchange (CEM) membranes; DC and CC are desalting and concentrating compartments, respectively. The points 1 and 1′ show where the tips of Luggin's capillaries are placed for measuring potential difference. (b) Schematic view of salt counterion (solid line) and co-ion (dashed line) concentration profiles in the diffusion boundary layer (DBL) of thickness δ near a CEM at different current densities. The DBL is divided in an electroneutral ($0 \le x \le \delta_1$) and a space charge ($\delta_1 < x \le 1$) regions. The intersection of the straight line extending the linear concentration profile in the electroneutral region with the x-axis gives the effective thickness of DBL (δ); λ is the thickness of quasi-equilibrium electric double layer. Adapted from Urtenov et al.[91]

fitted parameters for a system involving MK-40 and MA-40 membranes and concentrated LiCl aqueous solutions are gathered in Table 9.1.

The numerical values of parameters are well agreed with other data. Thus, the t_w/η value shows how many water moles are transported into the brine compartment with 1 mole of salt. This value should be close to the hydration

TABLE 9.1. Transport Characteristics of the MK-40/MA-40 Membrane Pair in LiCl Solutions[180]

η, %	$P_s \times 10^8$, m s^{-1}	$P_w \times 10^5$, m s^{-1}	t_w, $\frac{\text{mole } H_2O}{F}$
91 ± 6	2 ± 1	0.66 ± 0.13	10.5 ± 0.9

number of LiCl in concentrated water solutions, which conform to the membrane pore solution with the concentration close to 3–4 M. The hydration number of LiCl in 3 M solution is approximately equal to 12.[85]

It is shown[180] that the main membrane characteristics controlling ED concentration process are the permselectivity determining the value of η, and the electroosmotic permeability determining t_w. In a less degree, the process is affected by the diffusion and osmotic permeabilities.

9.4 CONCENTRATION POLARIZATION IN ED

9.4.1 Current-Induced Concentration Gradients

As noted above, the main functional property of IEMs is permselectivity toward the ions of a certain sign of charge (counterions). Namely, this feature determines the applications of this type of membranes in ED, enabling electrolyte concentration to decrease and increase in different ED compartments (Fig. 9.16a). However, the same property is the reason of restrictions in the mass transfer rate across IEMs in ED, which is referred to the current induced concentration polarization phenomenon. Thus, the understanding of concentration polarization is important for the successful application of IEMs and their improvement. In this section, we briefly consider this phenomenon.

When a direct current of density i is switched on across a membrane, during the first moments the current in the membrane is carried mainly by the counterions, while in the solution the contribution of both cations and anions is comparable. Hence, immediately after the switching, the migration flux of counterions through the membrane will be higher than their flux from the solution bulk to the interface. As a result, the concentration of counterions (it can be shown that the same concerns the co-ions) will decrease at one membrane side and increase at the other. The changes in concentrations will continue up to the moment when increasing with time diffusion transfer compensates completely the difference of migration fluxes in the solution and the membrane.

At any time, the flux density ingoing to the membrane/solution interface from the solution is equal to the flux density outgoing into the membrane bulk. This condition can be written as:

$$(J_i)_s = \left(-D\frac{\partial c_i}{\partial x} + \frac{it_i}{z_i F}\right)_s = \frac{iT_i}{z_i F}, \tag{9.45}$$

where $(J_i)_s$ is the flux density of ion i through the interface; the middle part of the Equation 9.45 refers to the solution: D is the electrolyte diffusion coefficient in solution, C_i and t_i are the concentration and transport number of ion i in solution; the right-hand part refers to the membrane: T_i is called the integral[13,181] or effective[52,182] transport number of this ion in the membrane. T_i is defined as the current fraction carried by ion i through the interface or the membrane in steady state under all forces applied:

$$T_i = \frac{z_i F (J_i)_s}{i}. \tag{9.46}$$

T_i can differ from the electromigration transport number in the membrane, t_i^{mb} (t_i in Eq. 9.7 written for a membrane) owing to the different migration contributions into the transfer: diffusion and convection. Nevertheless, if the external solution concentration is not too high, T_i is rather close to t_i^{mb}. Normally, commercial membranes are highly permselective to counterions[83]: the concentration of co-ions is much lower than that of counterions, hence, T_1 and t_i^{mb} verge toward 1.

Equation 9.45 expresses the condition of flux continuity at the interface, and is verified in unsteady and steady state. In steady state, the total flux density of any ion is the same at any point in the solution and the membrane.

The emergence of concentration gradients at membrane/solution interface under effect of external driving forces is called, following the International Union of Pure and Applied Chemistry (IUPAC) recommendations,[183] "concentration polarization." This term is used in electro- as well as in pressure-driven membrane processes.[10] In all cases, the reason of concentration polarization is that the membrane has the ability to transport some species more readily than the other(s): the retained species are concentrated at the interface while the concentration of transported species decreases. Thus, concentration polarization phenomenon is inherent to membrane separation processes. Note that sometimes concentration polarization is understood[184] as a complex of effects related to the formation of current-induced concentration gradients near a membrane (electrode) surface, including, in particular, the overlimiting current phenomenon.

According to classical electrochemistry, formation of concentration gradients near the surface of a membrane (or an electrode) results in the limitation of the current density, i. With increasing i, the electrolyte concentration at the interface, c_s, decreases (Fig. 9.16b). When c_s approaches zero (becomes much smaller than the bulk concentration, c^0), the current density reaches its limiting value (i_{lim}). The expression for i_{lim} is readily obtained from Equations 9.45 and 9.46, when writing the concentration gradient of the counterion (1) at the membrane surface as:

$$\left(\frac{\partial c_1}{\partial x}\right)_s = -\frac{c_1^0 - c_{1s}}{\delta}, \tag{9.47}$$

where δ is the thickness of the Nernst diffusion boundary layer (DBL) in the depleting solution. According to Equation 9.47, δ is the distance from the membrane to the intersection point of the tangent drawn to the concentration profile at the interface with the line corresponding to the bulk solution concentration. Substituting Equation 9.47 into Equation 9.45 and setting $c_{1s} = 0$ yields:

$$i_{\text{lim}} = \frac{FDc^0}{\delta(T_1 - t_1)}, \tag{9.48}$$

where $c^0 = z_+c_+^0 = -z_-c_-^0$ is the bulk electrolyte concentration in Eq L.$^{-1}$

Equation 9.48 was first obtained by Peers in 1956.[185]

Equation 9.48 assumes that the local electroneutrality condition is hold and no other charge carries besides salt anion and cation present in the solution. Within this approach, when i tends to its limiting value (i_{lim}), the potential drop over a membrane surrounded by two DBLs tends to infinity. However, in real membrane or electrode systems, the limiting current density can be exceeded in several times (Fig. 9.17) due to a complex of effects arising at the membrane (electrode) surface under the combined action of electric current

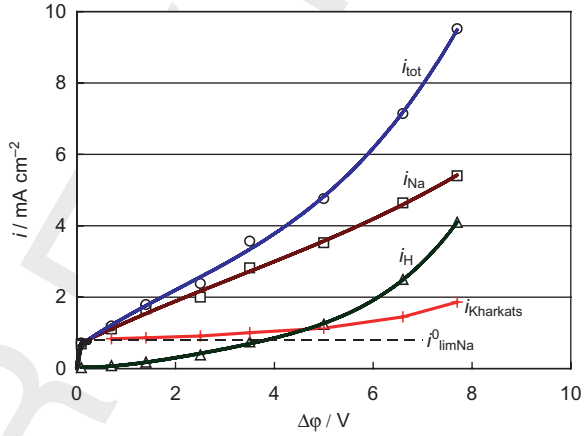

FIGURE 9.17. Current–voltage curves for a desalting compartment formed of a cation exchange membrane MK-40 and an anion exchange membrane MA-40 with 3 × 3 cm^2 of active membrane area and 1 mm of intermembrane space; the positions of measuring electrodes are shown in Figure 9.1a. A 0.002 M NaCl is flowing between the membranes with a velocity of 3.2 cm s^{-1}. The total current (i_{tot}) and partial currents of Na^+ (i_{Na}) and H^+ (i_{H}) ions through the MK-40 membrane, as well as the Kharkats current (i_{Kharkats}) and the limiting current density ($i^0_{\text{lim}\,Na}$), are shown; i_{tot}, i_{Na}, and i_{H} are experimental data,[188] i_{Kharkats} is calculated using Equation 9.36, and $i^0_{\text{lim}\,Na}$ is found by the intersection of tangents drawn to i_{tot} at $i = 0$ and at the inclined plateau region. Adapted from Urtenov et al.[91]

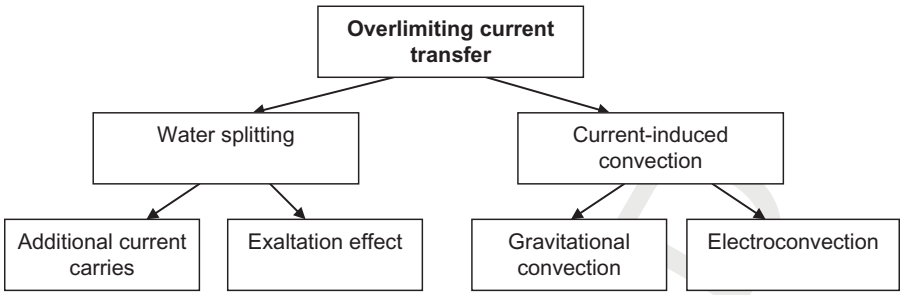

FIGURE 9.18. Scheme of overlimiting current transfer mechanisms.[203]

and concentration variations (produced by the same current) at the interface. In early period of ED, the use of underlimiting current was prescribed.[182,186] However, now the overlimiting current regimes are widely used in ED and especially in electrodeionization of diluted electrolyte solutions.[187–190] We will see below that the main effect responsible for the intensive overlimiting transfer is electroosmosis of the second kind,[191–193] also named induced-charge electroosmosis.[194,195] This effect is used in a number of nano- and microfluidic devices[118,124,194,196] such as electrokinetic micropumps.[197,198] Besides, intensive current regimes are applied in electrophoresis,[196] electrodeposition,[199] layering of colloid crystals on electrode surfaces,[200] and other domains related to separation science.[64,115,193]

9.4.2 Mechanisms of Overlimiting Current

In literature,[89,188,189,201–203] four effects explaining the overlimiting current transfer are discussed (Fig. 9.18). The first two are related to generation of H^+ (OH^-) ions (usually named "water splitting")[15,186] at the membrane/solution interface. The water splitting in membrane systems was observed by a number of researchers,[15,17,18,186,204,205] and for a long time the transfer of current by additional carriers, H^+ and OH^- ions, was considered as the main and often the only reason for the overlimiting conductance.[186] However, the generation of H^+ and OH^- ions causes another, less evident mechanism of overlimiting transfer, the exaltation effect, first studied by Kharkats.[206] The emergence of H^+ and OH^- ions near the interface disturbs the electric field that can increase (exalt) the salt counterion transfer: for example, the OH^- ions generated into the depleted diffusion layer adjacent to a cation exchange membrane attract the salt cations from the solution bulk toward the interface.

There are two other mechanisms of overlimiting conductance that contribute to salt counterion transfer. These are two types of current-induced convection, gravitational convection and electroconvection. They both provide additional mixing of depleted solution, in comparison with forced convection. This mixing is produced by local vortices resulting from the action of two volume forces different in nature.

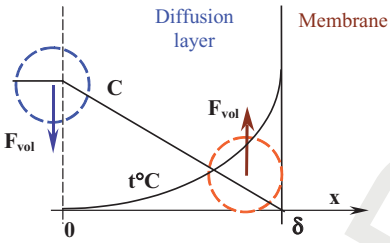

FIGURE 9.19. Scheme of gravitational convection.

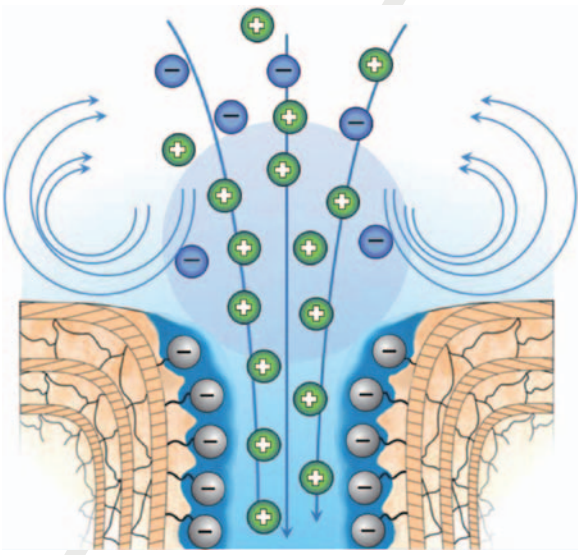

FIGURE 9.20. Scheme of electroconvection near the entrance in a membrane nanopore: the action of electric current on the space charge produces an excess in local pressure, which generates a pair of vortices. Adapted from Nikonenko et al.[203]

Gravitational convection develops due to the nonuniform distribution of solution density, which causes Archimedean volume force, $\mathbf{F}_{vol}$, bringing the liquid in motion (Fig. 9.19). Near the membrane, solution is more diluted then in the bulk. Moreover, its temperature is elevated due to Joule heat within a layer with high electric resistance. As a result, near the surface, the Archimedean buoyant force acts upon a parcel of fluid vertically upward, while in the bulk, the body force applied to a parcel of fluid acts in opposite direction. This couple of forces produces vortex motion of the fluid in the space near the membrane.

Electroconvection arises due to the action of the electric field on the electric space charge in the boundary depleted solution.[89,184,191,192] The mechanism of generation of a pair of vortices is shown in Figure 9.20. For this, a local increase in space charge density is needed. As the membrane surface is not electrically

homogeneous, this local increase is possible in different scales, from nanometer (shown in Fig. 9.20) to several tens of micrometer, in the case of heterogeneous membranes (Fig. 9.3b). Rubinstein and Zaltzman[184] have theoretically shown that electroconvective mixing develops even if the membrane surface is homogeneous, due to fluctuations at the wall. A slight distortion of membrane surface (making the surface waved) results in precipitation of the onset of overlimiting conductance and a respective increase of the current compared to those for a flat membrane.[184]

The structure of depleted DBL near an ion exchange membrane at different currents is shown in Figure 9.16b. Numerical and analytical solutions[89–91,184,207] have shown that the following three regions may be distinguished within the DBL (Fig. 9.16b). The quasi-electroneutral region of thickness δ_1 is next to the solution bulk. It is separated from the membrane surface by a space charge region (SCR), which adjoins the membrane surface and where the salt co-ion concentration is very small. The SCR may be divided into a migration zone (of thickness δ_2) and a quasi-equilibrium boundary layer (of thickness δ_3, denoted as λ in Fig. 9.16b). In the migration zone (which is absent at $i < i_{lim}$), the diffusion contribution to the counterion flux is negligible in comparison with the electromigration one. In the quasi-equilibrium zone, the diffusion and migration terms in Nernst–Planck's Equation 9.21 are high and have opposite signs, so that the J_1 term may be neglected, then c_1 and E are linked by the Boltzmann relation.

The fact that the DBL is distinctly divided into electroneutral and SCRs allows integration of flux equations in the region $0 \le x \le \delta'$ at $i \ge i_{lim}$, under the condition that the concentrations of all species are negligible at $x \le \delta$ in comparison with c_{10}. This integration conducts to an equation relating the flux density of counterion, J_1, with that of H^+ (OH^-) ions produced in the water splitting, J_w[52]:

$$J_1 = \frac{2D_1 c_{10}}{\delta'} + \frac{D_1}{D_w} J_w, \tag{9.49}$$

where subscript $_1$ refers to the salt counterion and $_w$ to the ion generated into the depleted solution in the course of water splitting (OH^- in the case of cation exchange membrane). Equation 9.49 is a generalization of Peers' Equation 9.48 and Kharkats' equation[206] deduced under the LEN assumption. δ' enters Equation 9.49 instead of δ in Peers' and Kharkats' equations. Thus δ' acts the role of the effective thickness of the DBL; geometrically, it is the distance from $x = 0$ to the point where the straight line following the counterion concentration profile in the electroneutral region cuts the x-axis (Fig. 9.16b). If we assume $\delta' = \delta_0$, where δ_0 is the DBL thickness formed near an "ideal" membrane not involving coupled convection (δ_0 may be calculated by the Leveque equation[88] for lamillar flow between two plates), the first term in Equation 9.49 gives a constant value, the limiting current density. In this case, the current density found by Equation 9.49 is called Kharkats' current.[91]

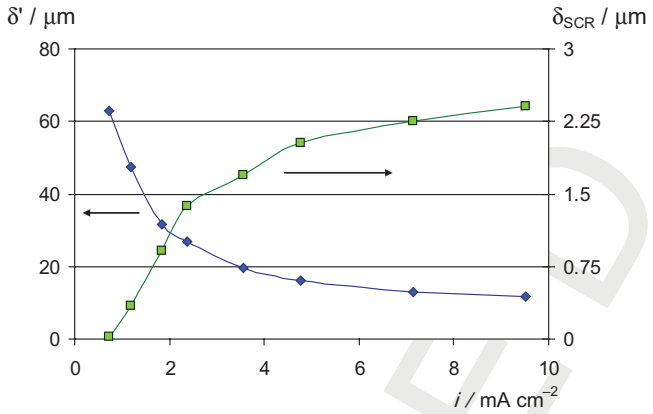

FIGURE 9.21. Effective thickness of the DBL (δ′) and the thickness of SCR (δ_{SCR}) as functions of the current density applied to the membrane system described in Figure 9.17. Adapted from Urtenov et al.[91]

Equation 9.49 shows that the overlimiting increase of the salt counterion flux density may be due to only two causes: a decrease in the effective thickness of the DBL, δ′, or an increase in the water splitting rate, J_w, which gives rise to the exaltation effect. The exaltation effect is rather low due to low value of the D_1/D_w ratio: it is about 0.25 in the case where ion $_1$ is Na^+, and $_w$ is OH^-.

When knowing the experimental values of J_1 and J_w , it is possible to evaluate δ′ from Equation 9.49 (Fig. 9.21).

The decrease in δ′ with increasing current density may be produced by current-induced convection mixing the boundary solution and shifting the outer edge of the DBL toward the membrane. As we mentioned above, this partial destruction of the DBL may be produced by gravitational convection or by electroconvection. The contribution of the gravitational convection in overlimiting current transfer is important when the variation in fluid density near the membrane and the spacing between the membranes (h) are high while the solution flow velocity (V) is low. Otherwise, when h, solution bulk concentration (c^0), and current density (i) are low, and V is high, gravitational convection is negligible. Theoretically, its contribution may be evaluated[208] via Rayleigh and Richardson numbers. In experiments, gravitation convection was negligible when $h < 1$ mm, $c^0 < 0.02$ M NaCl, and $V > 0.07$ cm s^{-1} [209] or $h < 6$ mm, $c^0 < 0.05$ M NaCl, and $V > 0.4$ cm s^{-1}.[203]

As opposed to gravitational convection, electroconvection is more intensive with diluting solution, since the EDL thickness as well as extended SCR[184] increases in this case. In the case of 0.002 M NaCl circulating through a short (3 cm) ED channel, the effective thickness of DBL can decrease to as low as 15 μm, under a rather strong, 8 V, potential difference over a pair cell (Fig. 9.21). The numerical calculation of the extended SCR thickness (by fitting the current–voltage curve[91] presented in Fig. 9.17) shows that this value may attain

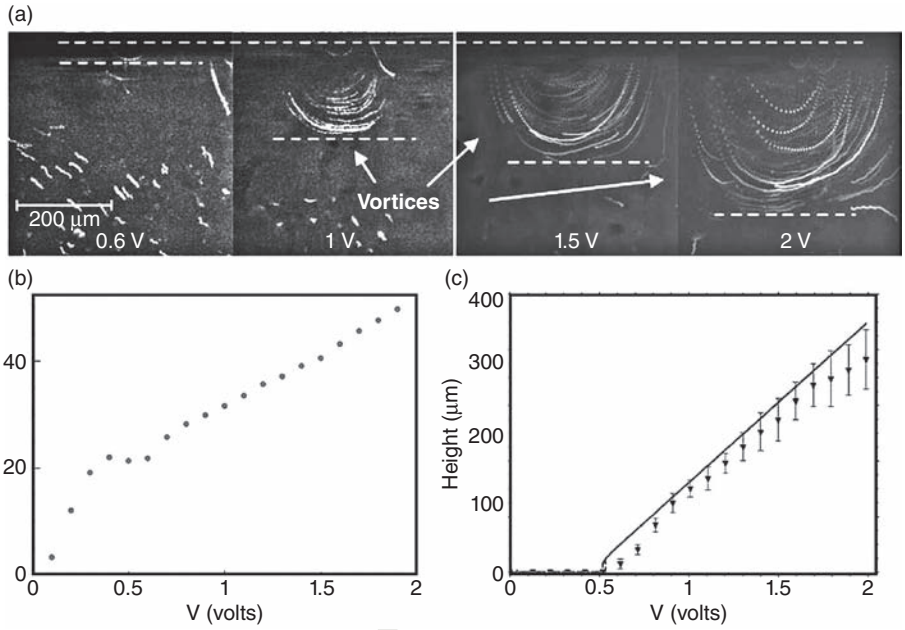

FIGURE 9.22. (a) Time-lapse snapshots of the experimental cell seeded with tracer particles showing "quasi-steady-state" streamlines. The membrane is situated at the top boundary of each image; the applied voltage (volts) is indicated. (b) Corresponding current–voltage curve. (c) The measured size of the vortical structures appearing at the limiting current density. Adapted from Rubinstein et al.[210]

few micrometers and become much higher than the equilibrium Debye length, λ (several nanometers).

The direct experimental observation of the nonequilibrium electroosmotic vortices together with simultaneous registration of current–voltage curves at overlimiting currents in an ED cell was realized by Rubinstein et al.[210] (Fig. 9.22). For the visualization, the authors have used tracers and a transparent cell. The membrane was positioned horizontally so that no gravitational convection appears: when a direct current is applied, a depleted DBL forms under a cation exchange membrane separated from a copper anode by a 0.005 M $CuSO_4$ solution. The heavier concentrated DBL is over the membrane under study.

9.5 RELATIONSHIPS BETWEEN ELECTROCHEMICAL BEHAVIOR OF ION EXCHANGE MEMBRANES AND THEIR BULK AND SURFACE STRUCTURE: MEMBRANE MODIFICATION

In previous sections, we have become acquainted with the structure and main properties of ion exchange membranes. A number of different membranes (about 50 kinds) are commercially available.[11,12] In spite of this variety, they

cannot satisfy increasing requirements of science and industry. For different separation processes, various properties are needed. Thus, in the case of deep water desalination by ED, the ability of the membrane to generate electroconvection is of great interest, while in the case of electrolyte concentration, the main desirable property is the ability to restrain the water transfer. For membranes used in fuel cells, the major characteristics are high electric conductivity, low gas permeability, high thermal stability, and low dependence of the conductivity on humidity.[21,211–213] In all cases, the membranes must have high selectivity toward counterion transport.

One of the most evident approaches for mass transfer improvement in membranes is their bulk and/or surface modification. Modification opens wide opportunities for preparation of membranes with different properties on the basis of a rather small number of commercially available membranes. A small amount of additive materials only slightly increases the costs of membrane production, hence this method is believed economically effective. We shall consider some examples of IEM modification aimed at improving their characteristics, necessary for different process.

9.5.1 Membrane Surface Modification

Membrane Profiling One of the first ideas of surface modification was membrane profiling in order to obtain relief (waved, undulated, or corrugated) surface.[189,214–217] The gain in mass transfer rate is determined by several effects. First, the active membrane area available for mass transfer increases. Second, there is an increase in fluid mixing by better hydrodynamic situation. Third, electroconvective mixing becomes more effective as the tangential component of driving force increases.[184,193] Fourth, the water splitting rate decreases, as the concentration polarization of the profiled membrane is lower. All these four effects are synergic in increasing mass transfer. As a result, the mass transfer coefficient, growing with diluting feed solution, can be up to 10 times higher than that in the same ED stack with conventional spacer (at 0.05 mM NaCl in the feed solution).[218]

Permselectivity among Different Ion Species Permselectivity of charged membranes toward ions of certain sign is their main property. It is possible to prepare membranes permselective to specific ion species. Permselectivity among ions of the same sign of charge in ED is governed by the difference in affinity of different ionic species with the membrane (ion exchange equilibrium constant) and the difference in the ionic mobility.[219] This specific permselectivity can be achieved by surface treatment of the membrane. One of the methods aiming at increasing membrane permselectivity toward monocharged counterions is surface coating with a thin ion exchange layer having a low concentration of fixed sites with the charge sign opposite to that of the fixed sites of the membrane bulk. Thus, a cation exchange membrane was coated with a (slightly charged) anion exchange layer, for example containing amines.[220,221] This thin layer serves as a barrier toward multicharged ions while

only slightly restraining the transfer of monocharged ones. This coating can be made, for example, by immersing a cation exchange membrane in a cationic weakly basic polyelectrolyte (such as polyethyleneimine) solution.[222] A relative transport number of the calcium to sodium ions dropped about 10 times during ED of a sodium chloride–calcium chloride solution. Moreover, this layer being a cationic surface-active agent can prevent the increase in the electric resistance of the membrane due to organic fouling.[222]

In Hu et al.,[223] quaternized chitosan was used as a cationic layer for surface modification of heterogeneous and homogeneous commercial cation exchange membranes to enhance their specific permselectivity. The transport number of the metallic multicharged cations was decreased significantly in binary systems (H^+/Zn^{2+} and H^+/Al^{3+}) after surface modification due to the electrostatic and steric barrier created by a thin chitosan layer.

Sata[219] has classified and reviewed methods resulting in obtaining specific permselectivity: (1) to vary cross-linkage of ion exchange membranes, (2) to form tight surface layers, (3) to decrease/increase hydrophilicity of the membrane surface by introducing specific ion exchange groups or to impregnate hydrophilic compounds, (4) to control permselectivity of anions by photoirradiation using membranes with a photoresponsive group, and (5) to control permselectivity through thermally responsive anion exchange membranes with temperature.

There is a large number of applications of IEMs with specific permselectivity.[219–226] Let us mention nitrate–chloride (drinking water denitrification),[224] fluoride–other anions (drinking water defluoridation),[225] chloride–sulfate (potable salt production from sea water)[226] separations, and others.[219]

Increasing Fouling Resistance Increasing fouling resistance can be obtained by the use of heterogeneous polyethylene-based anion exchange membranes modified by a hydrophilic anion exchange coating. The modified membranes showed a smaller fouling tendency than commercial ones in the desalination of recycled water.[227] Membrane modification with high molecular mass surfactants has mitigated fouling by organic compounds during ED of aqueous solutions.[228] Antifouling effect was also achieved by coating ion exchange membranes with a 12-μm-thick urethane acrylate layer.[229]

Lowering Water Splitting It is known that the rate of water splitting at the interface of anion exchange membranes generally is higher than that at the interface of cation exchange ones.[10,204,230] The reason is that secondary and tertiary amino groups often serving as ionogenic fixed sites in anion exchange membranes are strongly catalytically active in relation to water dissociation reaction.[15,17] Even when the ionogenic fixed sites are quaternary amino groups, sometimes these groups are not stable and transform into tertiary amino groups under the action of intensive electric current. An example is the case of AMX anion exchange membrane described by Choi and Moon.[231] High water splitting rate at anion exchange membrane in ED treatment of natural

waters leads not only to lower current efficiency, but some other nondesirable effects. In particular, in this case, the desalinating stream becomes acid that hampers the removal of weak acid anions, since they pass in nondissociated form. Moreover, alkalinization of the concentrating stream increases the risk of the hardness salts precipitation on the concentrating membrane surface.

It is possible to lower the water splitting rate by surface modification of anion exchange membrane. The case of modification of MA-40 with a strong polyelectrolyte solution is described in Pismenskaya et al.[232] The idea is to convert secondary and tertiary amino groups initially present in MA-40 membrane into quaternary ones, which are much less catalytically active toward water dissociation reaction.[15,17] Figure 9.23 shows the results of measurements of pH of the solution outgoing from ED desalination compartments formed by modified, MA-40M, or unmodified, MA-40, anion exchange membranes together with different cation exchange membranes, MK-40 or CMX (Neosepta®, Tokuyama Corporation, Shibuya, Japan). The rate of water splitting at the MA-40 membrane is higher than that at the MK-40 one. Hence, when the current density becomes equal or higher than i_{lim} (where the potential drop over a pair of the membranes with desalting solution between them, $\Delta\varphi$, is higher than 1 V), the pH of the outlet desalted solution becomes acidified: the amount of H^+ ions generated at the MA-40 membrane interface into the desalination compartment is higher than the amount of OH^- ions generated at the MK-40 interface. If MA-40 is replaced with the MA-40M membrane, there is no pH variation up to 3 i_{lim} (up to $\Delta\varphi \approx 9$ V), that is, the rate of water splitting at MA-40M is as low as that at MK-40. When MA-40M is used together with a CMX membrane, the desalted solution becomes alkalinized (in the interval between i_{lim} and 3 i_{lim}) because the rate of water splitting at CMX is higher than that at MA-40M. Note that the properties of modified MA-40M membrane was stable at list during 300 hours.[232]

Increasing Electroconvective Mixing According to classical physicochemical hydrodynamics,[233] the thickness of DBL and, hence, the limiting current density, Equation 9.48, are not functions of the surface properties. This is a consequence of the no-slip condition for the velocity at a solid wall. However, a strong correlation between the limiting (and overlimiting) current density and the contact angle on the membrane surface was established[203] (Fig. 9.24, Table 9.2). The contact angle, which is a measure of the surface hydrophobicity (determined in the swollen state 20 s after water drop application while the bottom of the membrane remains in contact with the equilibrium solution), increases in the range MK-40 < CMX < MK-40 + F < Nafion-117 (Table 9.2). The overlimiting mass transfer increases in the same range. Hence, the more the surface is hydrophobic, the higher the overlimiting mass transfer rate.

Note that the slip boundary condition was introduced by Navier in the form[166]:

$$u_{\text{slip}} = b\left(\partial V_y / \partial n\right)_{x=\delta}, \tag{9.50}$$

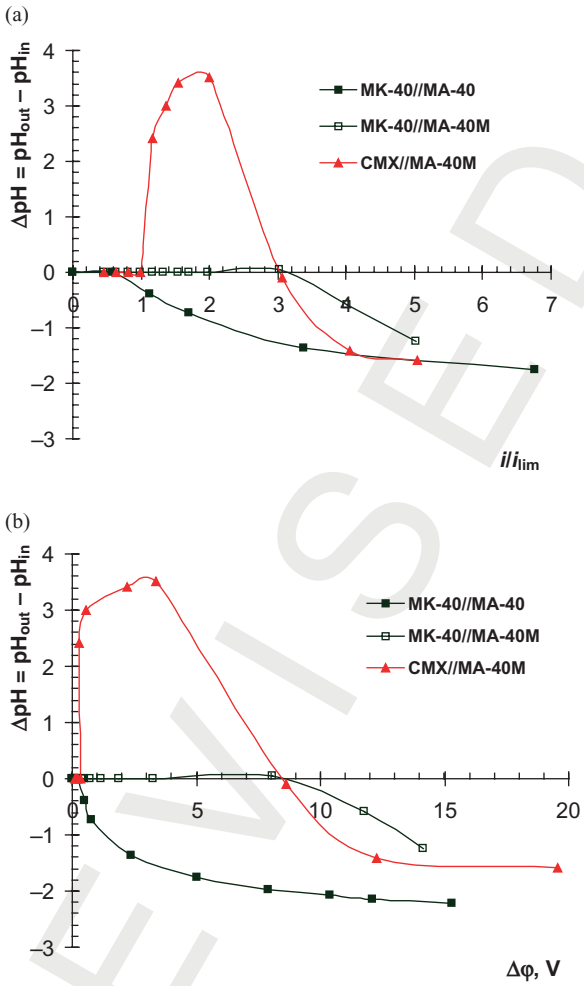

FIGURE 9.23. Difference of pH in the outlet and inlet solutions of the desalination compartment versus the current to limiting current ratio (a) and potential drop over a cell pair (b). $C = 0.005$ M; $h = 1$ mm; $S = 3 \times 3$ cm^2; $V = 1.6$ cm s^{-1}. Adapted from Pismenskaya et al.[232]

which relates the fluid tangential velocity u_{slip} at the surface and the shear strain rate normal to the surface, $\partial V_y/\partial n$, via the slip length b; the velocity of the surface is set to zero. $b = 0$ relates to the no-slip condition; u_{slip} increases with increasing b.

The nonslip condition is supported by macroscopic experiments, in particular, in electrochemistry when nonintensive current regimes are applied.[88] However, when fluid volumes are reduced, the impact of surface phenomena increases and the slip of fluid at the interface becomes important.[166,234] The slip

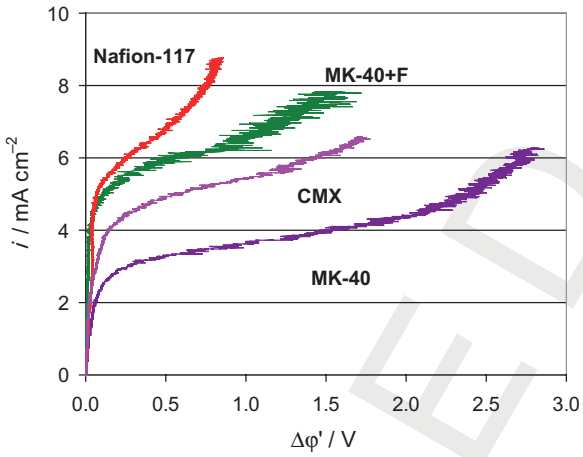

FIGURE 9.24. Current–voltage curves of MK-40, CMX, Nafion-117, and modified MK-40+F membranes in horizontal position with the depleted DBL under the membrane. $\Delta\varphi'$ is the corrected pd reduced by the ohmic contribution.[201] The limiting current density $i_{lim} = 2.7$ mA cm^{-2} is calculated using the Lévêque equation[88] deduced when applying the no-slip condition. Adapted from Nikonenko et al.[203]

TABLE 9.2. Contact Angles for Different Cation-Exchange Membranes[203]

Membrane	MK-40	CMX	MK-40+F	Nafion-117
Contact angle, degrees	39 ± 5	49 ± 3	53 ± 4	64 ± 4

velocity depends strongly on the degree of surface hydrophobicity. On the hydrophobic surface, there is a repulsion of water molecules, which causes a slip of the fluid over the surface.[235,236]

Slip velocities on both hydrophilic and hydrophobic surfaces have been studied using a variety of experimental techniques.[235–237] The values of slip length reported vary from several nanometers[236] to as high as several tens of micrometers.[237,238] Majumder et al[237] have found $b = 25$ μm from the pressure-driven flow rate measured through aligned multiwall carbon nanotubes incorporated in a membrane. The flow velocity normalized at 1 bar was found to be 25 cm s^{-1}, that is, four or five orders of magnitude faster than the evaluation by the Hagen–Poiseuille law. Hydrophobicity and, hence, the slip length can be significantly amplified by roughness and can reduce friction due to trapped nanobubbles.[239]

Obviously, the slip of fluid at hydrophobic surface takes place in the case of ion exchange membranes. This effect increases with increasing hydrophobicity, which explains the results presented in Figure 9.24.

The properties of MK-40 + F membrane present a particular interest. This membrane is prepared by casting a thin (of several micrometers thickness)

film of a sulfonated perfluorocarbon polymer on the surface of heterogeneous MK-40 membrane. The increase in the contact angle on the surface of the modified membrane is due to hydrophobic properties of the caste film. Note that besides increasing overlimiting current density, the modified membrane is characterized by lower water splitting[240,241] due to homogenization of the current lines distribution near the surface.[203]

9.5.2 Membrane Bulk Modification

Preparation and Properties of Organic/Inorganic Materials The membrane surface properties control mainly separation processes. However, in other cases, such as fuel cells, it is desired to modify all the membrane volumes, since when the membrane thickness is minimized, all the membrane volumes should be active.[212] Hybrid organic/inorganic materials are the main subject of investigations in this field.[213,242,243] Generally, these composite materials present high interest due to their extraordinary properties, electrical, mechanical, thermal, and others, which arise from the synergism between the properties of the components.[11,244]

First works in the field of organic/inorganic materials were devoted to the synthesis of a large class of sulfonate membranes on the base of layered zirconium phosphate containing organic chains with $-SO_3H$ group. Alberti et al.[245–247] have synthesized a large number of new sulfonate materials with high proton conductivity, which can be promising for fuel cells.[248,249] However, their mechanical properties are not very attractive for membrane applications.

The most simple and common way of polymer membrane modification is the use of small inorganic particles (mainly nanoparticles). They can be presented both by substances capable of generating mobile ions during dissociation or by inert compounds.[212,242] Among various types of inorganic components, which can be used for membrane modification, oxides of polyvalent elements (silicon, aluminum, zirconium) are used most frequently.

The modification of membrane materials by inorganic nanoparticles can be performed by two ways: first, by membrane casting from solutions containing finely dispersed additives[212,213] and second, by nanoparticle synthesis in the membrane matrix (*in situ*).[213,250–252] The first way is the most simple, but it does not always get successful results because finely dispersed particles can easily form aggregates. It reduces significantly the efficiency of membrane doping and sometimes results in the loss of mechanical strength and in macroporosity increase. Hence, high gas permeability is a typical defect of these membranes. Thus, the stabilization of their surface by various surfactants can be very attractive.[253,254]

On the other hand, the synthesis of nanoparticles may occur *in situ*, within the membrane matrix. The nanopores can uptake one of the initial reagents, for example, cations of polyvalent elements. After that, it is possible to carry out the further synthesis of nanoparticles in the same pores, using them for restriction of reaction volume and the size of formed particles. In this case the

pores play a role of nanoreactors. The pore walls can isolate the formed particles from each other and reduce the surface tension, providing thermodynamic stability of nanoparticles.

A review of the methods of organic/inorganic materials preparation is made by Xu.[11]

Note that modification of homogeneous ion exchange membranes (such as perfluorinated Nafion and MF-4SK membranes) by inorganic particles results in noticeable improvement of these membranes (both ion conductivity and selectivity are improved),[250,255–257] while it is not the case of heterogeneous membranes such as MK-40.[251,252] The reason is that heterogeneous membranes contain both micro- and macropores. Therefore, the size of acid zirconium phosphate particles (from X-ray data) in MK-40 is much higher than that in MF-4SK membrane (2–5 nm).

Nanocomposites on the basis of ion exchange membranes, containing nanoparticles of organic substances, were recently investigated. The most important additive of this type is polyaniline. Such composites can be obtained by aniline polymerization in membrane matrix (e.g., in Nafion),[258] as well as in their solutions with the subsequent casting.[259] In the latter case the size of polyaniline (or polyaniline/Nafion interpolymer) particles is not limited by the size of membrane pores and changes from several up to tens of nanometers depending on the concentration of solutions used for synthesis and way of membrane preparation.[259]

Composite membranes on the basis of MF-4SK and polyaniline possess mixed ion and electronic conductivity in the case of the bulk modification. Contribution of electronic conductivity can reach 60–70%, if polyaniline was obtained *in situ* in membrane matrix.[258] These composites have the mixed proton–electron conductivity, which keeps the high value, but the composite diffusion permeability in acid solution decreases after modification.[257] At the same time, proton conductivity of membranes obtained by casting after aniline polymerization in MF-4SK solution passes through the maximal value for low polyaniline concentration.[259] The increase in polyaniline content results in both decrease of proton conductivity and mechanical properties of membranes. The addition of small amounts of polyaniline results in the linkage of a part of protons, in an increase of defect concentration, and probably in improving of membrane microstructure. Further increase in polyaniline concentration results in the decrease in current carrier concentration (the protons are bonded with nitrogen by strong hydrogen bonds SO_3-H–N-). Large polyaniline particles can exclude some proton conductivity channels from transport process.[259] The morphology transitions inside of the nanostructure of the basic membrane lead to a decrease in the conductivity, diffusion, and electroosmotical permeability of surface modified by polyaniline composite materials.[257,259] The properties of the obtained samples depends on the way of the polyaniline intercalation. As a result, the samples of MF-4SK/polyaniline after surface modification proved themselves as quite efficient for ED concentration of salt solutions[260] and for fuel cells.[258]

Composite MF-4SK/polyaniline membranes have essentially changed diffusive permeability in comparison with the starting material. A reduction of water transport number is also noted. It can be explained by decrease in membrane hydrophilic property.[259]

Special attention should be given to the problem of asymmetry of transport processes in membrane materials. Membranes with asymmetric permeability have been obtained by oxide nanoparticles introduction with a gradient distribution. The difference in the diffusion permeability in opposite directions can achieve 40%.[255,256] Anisotropic composite membranes on the basis of MF-4SK and polyaniline[145,259,261] were also obtained. The asymmetry of diffusion permeability and ion conductivity was found for these membranes. Similar properties were obtained for MK-40 and MA-41 membranes modified by tetrabutylammonium or dodecyl sulfate.[262,263]

Between other approaches to form composite membranes, nonconducting polymers impregnation by molecules or nanoparticle of substances containing mobile ions can be mentioned.[212,213] In order to have the possibility to dissolve such additives, the polymer must contain electronegative atoms. Membranes on poly(ethylene oxide) $(\text{-CH}_2\text{-CH}_2\text{-O-})_n$ basis are often used for these purposes. Initial material has very low conductivity; however, the presence of a large number of oxygen atoms determines good solubility of various salts or acids in it. Their dissociation in membrane matrix provides high concentration of mobile ions and results in high ionic conductivity of such materials. Ion transfer in these materials takes place by means of cations motion from one group of electronegative atoms to another on a background of intensive segmental mobility of the polymer matrix providing reorganization of coordination polyhedrons. Such membranes with high lithium conductivity are often used in lithium batteries.[264–266]

Membrane materials can be doped by acids in order to increase proton conductivity as in the case of introduction of phosphoric acid into polybenzimidazole.[267,268] New membranes with high proton conductivity on the base of poly(vinyl alcohol) doped by phenol-sulfonic acids were also recently synthesized.[88,269]

Mechanism of the Increase in Ionic Conductivity of Polymer Membranes by Their Modification with Inorganic Nanoparticles The increase in ionic conductivity of composite materials was discovered by Liang.[270] This phenomenon can be attributed to the formation of additional defects, caused by the sorption processes at the phase boundary.[271,272] The optimal result should be achieved in the case of weak base (such as polyaniline) incorporation into Nafion membrane. The incorporation of small polyaniline amounts results in membrane conductivity increase. But if its concentration is more than 2 vol %, the membrane conductivity decreases with increasing polyaniline content. It is caused by the exception of too much carriers (protons) from the transfer process due to the sorption processes.

An increase in proton conductivity of hybrid membranes can be also achieved by incorporation of nanoparticles containing acid groups (acid zirconium phosphate).[252,256,273,274] In the last cases we can suppose that acid zirconium phosphate dissociation can increase carrier concentration. Similar results were obtained in the case of hydrophobic (metal) nanoparticles incorporation.[275] Moreover, Nafion-type membranes are strong acids[21] and the degree of dissociation of sulfonate groups is close to 100% in the hydrated state. Hence, the defect concentration (the oxonium ion in the frame of water molecules) is very high. Another suggestion, which is discussed in the literature, is the additional water molecules sorption by hydrophilic particles.[212] This can assist the proton transfer in membrane matrix according to the Grotthuss mechanism. But in the case of hydrophobic silver and polyaniline nanoparticles, the increase in proton conductivity cannot be explained by additional water sorption.

Proton diffusivities calculated from ^{1}H nuclear magnetic resonance (NMR) relaxation are mainly controlled by proton and water molecule migration in wide pores where most of the protons and water molecules are located.[276] These values are much higher than those calculated from membrane conductivity, since the latter are controlled by proton and water transfer through the narrow channels. The membrane modification by different dopants leads to the increase in ionic conductivity. At the same time, ^{1}H NMR relaxation rate in modified membranes can be both higher or lower in comparison with that of the unmodified samples.[276] This shows that the increase in proton conductivity can be attributed to the influence of incorporated nanoparticles on the size of narrow channels controlling ionic conductivity.

The formation of dopant nanoparticles takes place in the membrane pores. These particles occupy a part of the pore volume. The driving force of the pore expansion is osmotic pressure, which is determined mostly by the concentration of acid protons. The total amount of protons remains the same after modification, in the most cases. The amount of water molecules within the membrane matrix remains the same or even slightly increases after incorporation of hydrophilic particles. Incorporation of hydrophobic particles results in a decrease in water uptake by the modified membrane, but in this case, a noticeable pore volume increase can also be observed.[277]

Figure 9.25a,b shows the mechanism of the effect of nanoparticle growth within a large pore on the size of narrow channel linking two neighboring pores.[277] Expansion in the channel radius results in an increase in membrane ionic conductivity, which is controlled by proton transfer through such channels with low proton mobility. The activation energy of conductivity should decrease and approaches the activation energy for aqueous acidic solutions (5 kJ mol^{-1}).

Figure 9.25b,c shows that when the size of nanoparticles is not too high, they do not encumber all the space within a pore, however they allow an increase in channel radius. Further increase in nanoparticles volume (>3–4%

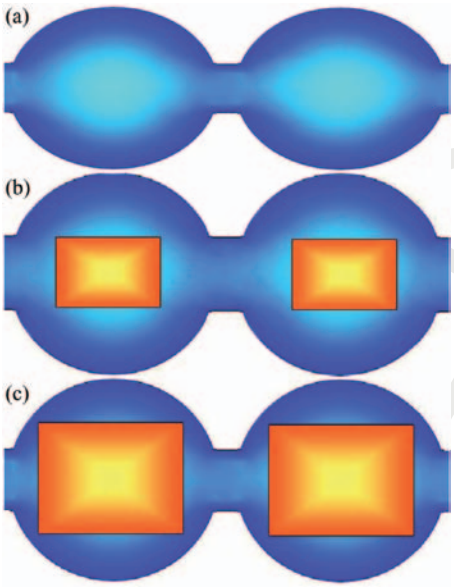

FIGURE 9.25. Scheme of pore structure for the (a) initial and (b, c) modified by nanoparticles membranes.

of total membrane volume) leads to essential encumbering of pore volume resulting in a decrease of conductivity and a growth of activation energy. The increase in nanoparticle volume up to 3–4 vol % leads also to a decrease in water uptake.[277]

Since a nanoparticle occupies the central part of a pore, the space available for free water molecules is found reduced. As a result, the volume fraction of bound water molecules making part of hydration shells increases. As well, the water activity increases, which leads to growing osmotic pressure, Equation 9.10, which is the cause of the increase in the pore size of modified membranes.

The dopant nature significantly affects the membrane conductivity. Thus, membranes doped with silica and zirconia are more conductive in comparison with the membranes doped with hydrophobic metallic particles. This effect is due to additional water sorption on the hydrophilic particle surface. Further conductivity increase can be achieved by simultaneous membrane modification by silica and phosphotungstic acid (PWA).[272,278] Most likely, the additional growth of proton conductivity can be explained by the increase in charge carrier (protons) concentration, which is accompanied by water uptake increase.

High proton conductivity at low humidity is mentioned among the main advantages of hybrid membranes.[212,279] A decrease in humidity results in partial membrane dehydration and in a dramatic decrease of pore volume.

The first advantage of the hybrid membranes in comparison with unmodified ones is that the pore and channel sizes in the first ones retains higher. But the main reason of low proton conductivity of membranes at low humidity is high distance between oxygen atoms participating in proton transfer. In hybrid membranes additional groups containing oxygen ions are incorporated into the membrane matrix. They also participate in the proton transfer process. These two facts results in the proton conductivity increase in hybrid materials at low humidity, which is very important for their application in fuel cells. And in the case of simultaneous membrane modification by silica and PWA, the effect of proton conductivity increase at low humidity became much more marked.[279] It means that the change of pores and channels size is important, but the nature of dopant particles is very important too. This fact makes the search of new approaches to membrane modification very promising.

ACKNOWLEDGMENTS

The chapter is prepared in the framework of the French–Russian laboratory "Ion-Exchange Membranes and Related Processes." We are grateful to CNRS, France, and RFBR, Russia, for financial support of this work.

ABBREVIATIONS AND SYMBOLS

Abbreviations

DBL	diffusion boundary layer
ED	electrodialysis
EDL	electrical double layer
IEM	ion exchange membrane
NPP	Nernst–Planck and Poisson (equations)
pd	potential difference
PFSA	perfluorosulfonated acid (ionomer)
TMS	Teorell–Meyer–Sievers (model)

Symbols

a_i, $a\pm$	ion and electrolyte molar activity, respectively
c_i	molar concentration of ion i
c^0, c_1^0	electrolyte and counterion concentration in the solution bulk, respectively
c_{1s}	counterion concentration at the membrane surface
d	thickness of the membrane

D electrolyte diffusion coefficient
D_i diffusion coefficient of ion i
F Faraday constant
f_1, f_2 volume fraction of gel and intergel regions in the membrane
i current density
i_{lim} limiting current density
J_i ionic flux density
J_v volume flux density
K equilibrium constant
L_D Debye length
L_p hydraulic permeability coefficient
p hydrostatic pressure
P membrane diffusion permeability
Q membrane ion exchange capacity
R universal gas constant
t time
t_i transport number of ion i
t_w water transport number
T absolute temperature
T_i effective transport number of ion i in the membrane
V velocity
$\bar{V}_s$ partial molar volume of electrolyte
$\bar{V}_w$ partial molar volume of water
x normal to membrane coordinate
$y\pm$ molar activity coefficient
z_i charge number of ion i

Greek Symbols

δ Nernst's diffusion layer thickness
δ' effective thickness of the DBL
κ electric conductivity, S m^{-1}
μ_i electrochemical potential
ν solution viscosity
π osmotic pressure
σ Staverman reflection coefficient
φ electric potential
Δ difference in a quantity
∇ gradient operator

Indices

A co-ion
^{g} superscript denoting that the quantity relates to the gel phase
i ionic species
^{s} superscript denoting that the quantity relates to the interstitial solution
w water, species produced by water splitting
1 counterion

REFERENCES

1. S. F. Timashev. *Physical Chemistry of Membrane Process*. Ellis Horwood Series in Physical Chemistry. Ellis Horwood, New York, 1991.
2. B. Alberts, A. Johnson, J. Lewis, et al. *Molecular Biology of the Cell*. Garland Science, New York, 2002.
3. H. Lodish, A. Berk, L. S. Zipursky, et al. *Molecular Cell Biology*. Scientific American Books, New York, 2004.
4. S. J. Singer and G. L. Nicolson. *Science* **1972**, 175, 720.
5. D. Evans and H. Wennerstrom. *The Colloidal Domain: Where Physics, Chemistry, Biology, and Technology Meet*. Wiley, New York, 1999.
6. A. Pohorille and M. A. Wilson. *Cell Mol Biol Lett* **2001**, 6, 369.
7. E. Gouaux and R. Mackinnon. *Science* **2005**, 310 (5753), 1461.
8. M. H. Cordes, A. R. Davidson, R. T. Sauer. *Curr Opin Struct Biol* **1996**, 6 (1), 3.
9. B. Hille. *Ion Channels of Excitable Membranes*. Sinauer Associates, Sunderland, MA, 2001.
10. H. Strathmann. *Ion-exchange Membrane Separation Processes*. Membrane Science and Technology Ser. 9. Elsevier, Amsterdam, 2004.
11. T. Xu. *J Membr Sci* **2005**, 263, 1.
12. R. K. Nagarale, G. S. Gohil, V. K. Shahi. *Adv Colloid Interface Sci* **2006**, 119, 97.
13. F. Hellferich. *Ion Exchange*. McGraw-Hill, New York, 1962.
14. G. E. Molau. *J Membr Sci* **1981**, 8, 309.
15. R. Simons. *Electrochim Acta* **1984**, 29, 151.
16. R. Simons. *J Membr Sci* **1993**, 82, 45.
17. V. I. Zabolotskii, N. V. Shel'deshov, N. P. Gnusin. *Russ Chem Rev* **1988**, 57, 801.
18. H. Strathmann, J. J. Krol, H. J. Rapp, et al. *J Membr Sci* **1997**, 125, 123.
19. K. A. Mauritz, D. A. Mountz, D. A. Reuschle, et al. *Electrochim Acta* **2004**, 50, 565.
20. K. A. Mauritz and R. B. Moore. *Chem Rev* **2004**, 104, 4535.
21. K. D. Kreuer, S. Paddison, E. Spohr, et al. *Chem Rev* **2004**, 104, 4637.
22. A. Eisenberg. *Macromolecules* **1970**, 3, 147.
23. T. D. Gierke and W. Y. Hsu. The cluster-network model of ion clustering in perfluorosulfonated membranes. A. Eisenberg, H.L. Yeager. Proceedings of the ACS Symposium on Perfluorinated Ionomer Membranes. Washington, 1982.

YU

24. E. J. Roche, M. Pinéri, R. Duplessix. *J Polym Sci Polym Phys Ed* **1982**, 20, 107.
25. I. M. Shiryaeva and A. I. Victorov. *Fluid Phase Equilibria* **2001**, 180, 115.
26. G. Gebel. *Polymer* **2000**, 41, 5829.
27. L. Rubatat, A. L. Rollet, G. Gebel, et al. Evidence of Elongated Polymeric Aggregates in Nafion. *Macromolecules* **2002**, 35, 4050.
28. D. Y. Galperin and A. R. Khokhlov. *Macromol Theory Simul* **2006**, 15, 137.
29. T. D. Gierke, G. E. Munn, F. C. Wilson. *J Polym Sci , Polym Phys Ed* **1981**, 19, 1687.
30. M. W. Verbrugge and R. F. Hill. *J Electrochem Soc* **1990**, 137 (3), 886.
31. Y. K. Tovbin and N. F. Vasutkin. *Colloids Surf A Physicochem Eng Aspects* **1999**, 158, 385.
32. H. G. Haubold, T. Vad, H. Jungbluth, et al. *Electrochim Acta* **2001**, 46, 1559.
33. A. L. Rollet, O. Diat, G. Gebel. *J Phys Chem* **2002**, 106, 3033.
34. M. V. Fedorov and A. A. Kornyshev. *Electrochim Acta* **2008**, 53 (23), 6835.
35. J. Fimrite, H. Struchtrup, N. J. Djilali. *J Electrochem Soc* **2005**, 152, A1804.
36. B. Corry, S. Kuyucak, S. H. Chung. *Chem Phys Lett* **2000**, 320, 35.
37. M. H. Litt. *Polym Prepr* **1997**, 38, 80.
38. K. D. Kreuer. *J Membr Sci* **2001**, 185, 29.
39. B. Loppinet, G. Gebel, C. E. Williams. *J Phys Chem* **1997**, 101, 1884.
40. S. Schlick, G. Gebel, M. Pineri, F. Volino. *Macromolecules* **1991**, 24, 3517.
41. S. J. Paddison, G. Bender, K. D. Kreuer, et al. *J New Mater Electrochem Syst* **2000**, 3, 293.
42. V. Saarinen, K. D. Kreuer, M. Schuster, et al. *Solid State Ionics* **2007**, 178, 533.
43. L. Chaabane, G. Bulvestre, C. Larchet, et al. *J Membr Sci* **2008**, 323, 167.
44. V. M. Barragan, J. P. G. Villaluenga, M. P. Godino, et al. *J Power Sources* **2008**, 185, 822.
45. S. J. Paddison, L. R. Pratt, T. A. Zawodzinski Jr. *J New Mater Electrochem Syst* **1999**, 2, 183.
46. Y. M. Volfkovich, V. S. Bagotzky, V. E. Sosenkin, et al. *Colloids Surf A Physicochem Eng Asp* **2001**, 187–188, 349.
47. N. P. Berezina, N. A. Kononenko, O. A. Dyomina, et al. *Adv Colloid Interface Sci* **2008**, 139 (1–2), 3.
48. Y. Mizutani. *J Membr Sci* **1990**, 49, 121–144.
49. J. J. Krol, M. Wessling, H. Strathmann. *J Membr Sci* **1999**, 162, 155.
50. P. Kofstad. *Nonstoichiometry. Diffusion and Electrical Conductivity in Binary Metal Oxides*. Wiley-Interscience, New York, 1972.
51. R. P. Buck. *J Membr Sci* **1984**, 17, 1.
52. V. I. Zabolotsky and V. V. Nikonenko. *Ion Transport in Membranes (in Russian)*. Nauka, Moscow, 1996.
53. N. Agmon. *Chem Phys Lett* **1995**, 244, 456.
54. J. A. Elliott and S. J. Paddison. *Phys Chem Chem Phys* **2007**, 9 (21), 2602.
55. M. Esai Selvan, D. J. Keffer, S. Cui, et al. *Mol Simul* **2010**, 36 (7–8), 568.
56. C. K. Knox and G. A. Voth. *J Phys Chem B* **2010**, 114, 3205.
57. A. A. Kornyshev, A. M. Kuznetsov, E. Spohr, et al. *J Phys Chem* **2003**, 107, 3351.

YU

58. S. Paddison and J. Annu. *Rev Mater Res* **2003**, 33, 289.
59. G. Pourcelly, A. Oikonomou, H. D. Hurwitz, et al. *J Electroanal Chem* **1990**, 287, 43.
60. R. Zallen. *The Physics of Amorphous Solids*. Wiley Interscience, New York, 1998.
61. V. I. Volkov, Y. A. Dobrovolsky, M. S. Nurmiev, et al. *Solid State Ionics* **2008**, 179 (1–6), 148.
62. N. Lakshminarayanaiah. *Transport Phenomena in Membranes*. Academic Press, New York, 1969.
63. K. Konturri, L. Murtomäki, J. A. Manzanares. *Ionic Transport Processes in Electrochemistry and Membrane Science*. Oxford University Press, New York, 2008.
64. A. B. Yaroslavtsev, V. V. Nikonenko, V. I. Zabolotsky. *Russ Chem Rev* **2003**, 72, 393.
65. A. Z. Weber and J. Newman. *Top Appl Phys* **2009**, 113, 157.
66. C.-Y. Wang. *Chem Rev* **2004**, 104, 4727.
67. D. Kondepudi and I. Prigogine. *Modern Thermodynamics—From Heat Engines to Dissipative Structures*. John Willey & Sons, New York, 1999.
68. S. R. Caplan and A. Essig. *Bioenergetics and Linear Nonequilibrium Thermodynamics*. Harvard University Press, Cambridge, 1983.
69. K. S. Spiegler. *Trans Faraday Soc* **1958**, 54, 1408.
70. V. I. Zabolotsky and V. V. Nikonenko. *J Membr Sci* **1993**, 79, 181.
71. O. Kedem and A. Katchalsky. *J Gen Physiol* **1961**, 45, 143.
72. A. Narebska, S. Koter, W. Kujawski. *Desalination* **1984**, 51, 3.
73. K. S. Spiegler and O. Kedem. *Desalination* **1966**, 1, 311.
74. B. Auclair, V. Nikonenko, C. Larchet, et al. *J Membr Sci* **2002**, 195, 89.
75. O. Kedem and A. Katchalsky. *Trans Faraday Soc* **1963**, 59, 1918.
76. P. Meares. *J Membr Sci* **1981**, 8, 295.
77. E. A. Mason and H. K. Lonsdale. *J Membr Sci* **1990**, 51, 1.
78. S. Koter, W. Kujawski, I. Koter. *J Membr Sci* **2007**, 297, 226.
79. O. Kedem and M. Perry. *J Membr Sci* **1983**, 14, 249.
80. A. Narebska and S. Koter. *Electrochim Acta* **1993**, 38, 815.
81. N. P. Gnusin, N. P. Berezina, N. A. Kononenko, et al. *J Membr Sci* **2004**, 243, 301.
82. C. Larchet, B. Auclair, V. Nikonenko. *Electrochim Acta* **2004**, 49, 1711.
83. C. Larchet, L. Dammak, B. Auclair, et al. *New J Chem* **2004**, 28, 1260.
84. C. R. Paterson and C. R. Gardner. *J Chem Soc* **1971**, 2254.
85. R. A. Robinson and R. H. Stokes. *Electrolyte Solutions*. Butterworths, London, 1959.
86. L. Lebrun, E. Da Silva, G. Pourcelly, et al. *J Membr Sci* **2003**, 227, 95.
87. R. Lteif, L. Dammak, C. Larchet, et al. *Eur Polym J* **2001**, 37, 627.
88. J. S. Newman. *Electrochemical Systems*. Prentice Hall, Englewood Cliffs, NJ, 1973.
89. B. Zaltzman and I. Rubinstein. *J Fluid Mech* **2007**, 579, 173.
90. K. T. Chu and M. Z. Bazant. *SIAM J Appl Math* **2005**, 65, 1485.
91. M. A.-K. Urtenov, E. V. Kirillova, N. M. Seidova, et al. *J Phys Chem B* **2007**, 111, 14208.

YU

92. R. Schlögl. *Stofftransport Durch Membranen*. Steinkopff-Verlag, Darmstadt, 1964.
93. P. Turq, J. Barthel, M. Chemla. *Transport, Relaxation, and Kinetic Processes in Electrolyte Solutions*. Springer-Verlag, Berlin, 1992.
94. G. Pourcelly, P. Sistat, A. Chapotot, et al. *J Membr Sci* **1996**, 110, 69.
95. S. Bandini and L. Bruni. Transport phenomena in nanofiltration membranes. In *Comprehensive Membrane Science and Engineering*, E. Drioli, L. Giorno, eds. Elsevier Science, 2010; Vol. 2, p. 67.
96. G. Jonsson and F. Macedonio. Fundamentals in reverse osmosis. In *Comprehensive Membrane Science and Engineerining*, E. Drioli, L. Giorno, eds. Elsevier Science, 2010; Vol. 2, p. 1.
97. M. Caputo and C. Cametti. *J Theor Biol* **2008**, 254, 697.
98. T. Teorell. *Proc Soc Exp Biol Med* **1935**, 33, 282.
99. K. H. Meyer and J. F. Sievers. *Helv Chim Acta* **1936**, 19, 649.
100. E. Glueckauf and R. E. Watts. *Proc R Soc Lond* **1962**, A 268, 339.
101. Y. Tanaka. Theory of Teorell, Meyer and Sievers (TMS Theory). Chapter 4 in: *Membr Sci Technol* **2007**, 12, 59.
102. V. V. Nikonenko, K. A. Lebedev, V. I. Zabolotsky, et al. *Eur Polym J* **1997**, 33, 1057.
103. A. V. Sokirko, J. A. Manzanares, J. Pellicer. *J Colloid Interface Sci* **1994**, 168, 32.
104. A. A. Moya and J. A. Moleón. *J Electroanal Chem* **2010**, 647, 53.
105. S. Levine, J. R. Marriott, G. Neale, et al. *J Colloid Interface Sci* **1975**, 52, 136.
106. S. Koter. *J Membr Sci* **2002**, 206 (1–2), 201.
107. V. Garcia-Morales, J. Cervera, J. A. Manzanares. *J Electroanal Chem* **2007**, 599, 203.
108. A. G. Guzmán-Garcia, P. N. Pintauro, M. V. Verbrugge. *AIChE J* **1990**, 36, 1061.
109. X. Lefebvre and J. Palmeri. *J Phys Chem* **2005**, 109, 5525.
110. A. Yaroshchuk, Y. Boiko, A. Makovetskiy. *Langmuir* **2009**, 25, 9605.
111. A. Szymczyk, H. C. Zhu, B. Balannec. *J Phys Chem B* **2010**, 114, 10143.
112. R. Zallen. *The Physics of Amorphous Solids*. John Wiley & Sons, New York, 1983.
113. M. Eikerling and A. A. Kornyshev. *J Electroanal Chem* **2001**, 501, 196.
114. A. Mansouri, C. Scheuerman, S. Bhattacharjee, et al. *J Colloid Interface Sci* **2005**, 292, 567.
115. A. Höltzel and U. Tallarek. *J Sep Sci* **2007**, 30, 1398.
116. Y. Yang and P. N. Pintauro. *Ind Eng Chem Res* **2004**, 43, 2957.
117. R. B. Schoch, J. Han, P. Renaud. *Rev Mod Phys* **2008**, 80, 839.
118. J. de Jong, R. G. H. Lammertink, M. Wessling. *Lab Chip* **2006**, 6, 1125.
119. E. H. Cwirko and R. G. Carbonell. *J Membr Sci* **1992**, 67, 227.
120. A. Szymczyk, P. Fievet, B. Aoubiza, et al. *J Membr Sci* **1999**, 161, 275.
121. P. Commer, A. Cherstvy, E. Spohr, et al. *Fuel Cells* **2003**, 2, 127.
122. R. Paul and S. J. Paddison. *J Chem Phys* **2005**, 123, 224704.
123. M. Z. Bazant, M. S. Kilic, B. Storey, et al. *Adv Colloid Interface Sci* **2009**, 152, 48.
124. M. Z. Bazant and T. M. Squires. *Curr Opin Colloid Interface Sci* **2010**, 15, 203.
125. N. P. Berezina and L. V. Karpenko. *Rus Colloid J* **2000**, 62, 676.
126. M. M. Dubinin. *Russ Chem Rev* **1982**, 51, 605.

127. N. P. Gnusin, V. D. Grebenyuk, M. V. Pevnitskaya. *Electrochemistry of Ion Exchangers*. Nauka, Novosibirsk, 1972.
128. S. Mafé, J. A. Manzanares, P. Ramirez. *Phys Chem Chem Phys* **2003**, 5, 376.
129. A. G. Rojo and H. E. Roman. *Phys Rev* **1988**, 37, 3696.
130. H. L. Duan, B. L. Karihaloo, J. Wang, et al. *Phys Rev B* **2006**, 73 (17), 174203.
131. V. M. Starov and V. G. Zhdanov. *Adv Colloid Interface Sci* **2008**, 137 (1), 2.
132. R. Pal. *Mater Sci Eng A* **2008**, 498 (1–2), 135.
133. M. Zhdanov. *Geophysics* **2008**, 73 (5), F197.
134. S. I. Vasin, A. N. Filippov, V. M. Starov. *Adv Colloid Interface Sci* **2008**, 139, 83.
135. J. C. Maxwell. *Treatise on Electricity and Magnetism*. Clarendon, Oxford, 1873.
136. R. Wodzki and A. Narebska. *Angew Macromol Chem* **1980**, 88, 149.
137. J. S. Mackie and P. Meares. *Proc R Soc Lond A* **1955**, 232, 498A.
138. N. P. Gnusin, V. I. Zabolotskii, V. V. Nikonenko, et al. *Zh Fiz Khim* **1980**, 54, 1518.
139. W. Y. Hsu, T. D. Gierke, C. J. Molnar. *Macromolecules* **1983**, 16, 1945.
140. N. N. Belaid, B. Ngom, L. Dammak, et al. *Eur Polym J* **1999**, 35, 879.
141. M. T. Bryk, V. I. Zabolotskii, I. D. Atamanenko, et al. *Sov J Water Chem Technol* **1989**, 11, 14.
142. N. Pismenskaya, E. Laktionov, V. Nikonenko, et al. *J Membr Sci* **2001**, 181, 185.
143. P. V. Vyas, P. Ray, S. K. Adhikary, et al. *J Colloid Interface Sci* **2003**, 257, 127.
144. X. T. Le, T. H. Bui, P. Viel, et al. *J Membr Sci* **2009**, 340, 133.
145. A. N. Filippov, V. M. Starov, N. A. Kononenko, et al. *Adv Colloid Interface Sci* **2008**, 139 (1–2), 29.
146. K. A. Lebedev, V. V. Nikonenko, et al. *Sov Electrochem* **1987**, 23, 459.
147. X. T. Le. *Adv Colloid Interface Sci* **2008**, 325, 215.
148. N. P. Berezina, N. Gnusin, O. Dyomina, et al. *J Membr Sci* **1994**, 86, 207.
149. L. X. Tuan and C. Buess-Herman. *Chem Phys Lett* **2007**, 434, 49.
150. C. Larchet, S. Nouri, B. Auclair, et al. *Adv Colloid Interface Sci* **2008**, 139, 45.
151. P. Huguet, T. Kiva, O. Noguera, et al. *New J Chem* **2005**, 29, 955.
152. V. I. Zabolotskii, V. V. Nikonenko, O. N. Kostenko, et al. *Zh Fiz Khim* **1993**, 67, 2423.
153. A. Elattar, A. Elmidaoui, N. Pismenskaia, et al. *J Membr Sci* **1998**, 143, 249.
154. J.-H. Choi, S.-H. Kim, S.-H. Moon. *Adv Colloid Interface Sci* **2001**, 241, 120.
155. L. X. Tuan, M. Verbanck, C. Buess-Herman, et al. *J Membr Sci* **2006**, 284, 67.
156. J. P. G. Villaluenga, V. M. Barragán, M. A. Izquierdo-Gil, et al. *J Membr Sci* **2008**, 323, 421.
157. M. Kumar, S. Singh, V. K. Shahi. *J Phys Chem B* **2010**, 114, 198.
158. A. Z. Weber and J. Newman. *J Electrochem Soc* **2006**, 153, A2205.
159. M. Eikerling. *J Electrochem Soc* **2006**, 153, E58–E70.
160. S. Litster, C. R. Buie, T. Fabian, et al. *J Electrochem Soc* **2007**, 154 (10), B1049–B1058.
161. A. J. B. Kemperman, ed. *Handbook on Bipolar Membrane Technology*. Twente University Press, Enschede, 2000.

YU

162. K. D. Kreuer. *Solid State Ionics* **1997**, 97, 1.
163. T. A. Zawodzinski, T. E. Springer, J. Davey, et al. *J Electrochem Soc* **1993**, 140, 1981.
164. S. Hietala, S. L. Maunu, F. Sundholm. *J Polym Sci B Polym Phys* **2000**, 38, 3277.
165. P. Thompson and S. Troian. *A General Boundary Condition for Liquid Flow at Solid Surfaces*. Nature, London, 1997.
166. M. Z. Bazant and O. I. Vinogradova. *J Fluid Mech* **2008**, 613, 125.
167. F. Meier and G. Eigenberger. *Electrochim Acta* **2004**, 49, 1731.
168. M. Eikerling, Y. I. Kharkats, A. A. Kornyshev, et al. *J Electrochem Soc* **1998**, 145, 2684.
169. T. A. Zawodzinski, J. Davey, J. Valerio, et al. *Electrochim Acta* **1995**, 40, 297.
170. G. Xie and T. Okada. *Electrochim Acta* **1996**, 41, 1569.
171. T. Okada, G. Xie, O. Gorseth, et al. *Electrochim Acta* **1998**, 43, 3741.
172. A.-L. Rollet, G. Gebel, J.-P. Simonin, et al. *J Polym Sci* **2001**, 39 (2), 548.
173. M. Tasaka, Y. Kondo, M. Nagasawa. *J Phys Chem* **1969**, 73, 3181.
174. J. P. García-Villaluenga, B. Seoane, V. M. Barragán. *J Colloid Interface Sci* **2003**, 263, 217.
175. R. Schlögl. *Z Phyzik Chem (Frankfurt)* **1955**, 3, 73.
176. H. Fujita and Y. Kobatake. *J Colloid Interface Sci* **1968**, 27, 609.
177. O. Bobreshova, I. Aristov, P. Kulintsov, et al. *J Membr Sci* **2000**, 177, 201.
178. N. V. Shel'deshov, V. V. Chaika, V. I. Zabolotskii. *Russ J Electrochem* **2008**, 44, 1036.
179. A. N. Filippov, S. I. Vasin, V. M. Starov. *Colloids Surf A* **2006**, 282–283, 272.
180. V. I. Zabolotskii, A. A. Shudrenko, N. P. Gnusin. *Sov Electrochem* **1988**, 24, 689.
181. J. Manzanares and K. Kontturi. Diffusion and migration. In *Encyclopedia of Electrochemistry. V. 2. Interfacial Kinetics and Mass Transport*, A. J. Bard, M. Stratmann, E. J. Calvo, eds. VCH-Wiley, Weinheim, 2003.
182. S.-T. Hwang and K. Kammermeyer. *Membranes in Separation*. Wiley, New York, 1975.
183. W. J. Koros, Y. H. Ma, T. Shimidzu. *Pure Appl Chem* **1996**, 68, 1479.
184. I. Rubinstein and B. Zaltzman. *Phys Rev E* **2000**, 62, 2238.
185. A. M. Peers. *Discuss Faraday Soc* **1956**, 21, 124.
186. C. Forgacs, N. Ishibashi, J. Leibovitz, et al. *Desalination* **1972**, 10, 181.
187. T. A. Davis, V. Grebenyuk, O. Grebenyuk. *Membrane Technology in Chemical Industry*, S. P. Nunes, K.-V. Peinemann, eds. Wiley-VCH, Weinheim, 2001.
188. V. I. Zabolotsky, V. V. Nikonenko, N. D. Pismenskaya, et al. *Sep Purif Technol* **1998**, 14, 255.
189. J. Balster, M. H. Yildirim, D. F. Stamatialis, et al. *J Phys Chem B* **2007**, 111, 2152.
190. J. Lu, Y.-X. Wang, J. Zhu. *Electrochim Acta* **2010**, 55, 2673.
191. S. S. Dukhin. *Adv Colloid Interface Sci* **1991**, 35, 173.
192. N. A. Mishchuk and S. S. Dukhin. *Interfacial Electrokinetics and Electrophoresis*, A. Delgado, ed. Marcel Dekker, New York, 2002.
193. N. A. Mishchuk. *Adv Colloid Interface Sci* **2010**, 160 (1–2), 16.
194. T. M. Squires and M. Z. Bazant. *J Fluid Mech* **2004**, 509, 217.
195. F. C. Leinweber and U. Tallarek. *J Phys Chem B* **2005**, 109, 21481.

YU

196. N. A. Mishchuk, T. Heldal, T. Volden, et al. *Electrophoresis* **2009**, 30, 3499.
197. A. Ajdari. *Phys Rev E* **2000**, 6, 45.
198. D. Kim, J. D. Posner, J. G. Santiago. *Sens Actuators A* **2008**, 141, 201.
199. V. M. Volgin and A. D. Davydov. *Electrochim Acta* **2004**, 49, 365.
200. M. Trau, D. A. Saville, I. A. Aksay. *Science* **1996**, 272, 706.
201. E. I. Belova, G. Y. Lopatkova, N. D. Pismenskaya, et al. *J Phys Chem B* **2006**, 110, 13458.
202. V. A. Shaposhnik, V. I. Vasil'eva, O. V. Grigorchuk. *Adv Colloid Interface Sci* **2008**, 139, 74.
203. V. V. Nikonenko, N. D. Pismenskaya, E. I. Belova, et al. *Adv Colloid Interface Sci* **2010**, 160, 101–123.
204. J. J. Krol, M. Wessling, H. Strathmann. *J Membr Sci* **1999**, 162, 145.
205. Y. Tanaka. *J Membr Sci* **2010**, 350, 347.
206. Y. I. Kharkats. *Sov Electrochem* **1985**, 21, 917.
207. J. A. Manzanares, W. D. Murphy, S. Mafé, et al. *J Phys Chem* **1993**, 97, 8524.
208. I. Rubinstein, B. Zaltzman, O. Kedem. *J Membr Sci* **1997**, 125 (1), 17.
209. V. I. Zabolotsky, V. V. Nikonenko, N. D. Pismenskaya. *J Membr Sci* **1996**, 119 (2), 171–181.
210. S. M. Rubinstein, G. Manukyan, A. Staicu, et al. *Phys Rev Lett* **2008**, 101, 236101.
211. M. A. Hickner, H. Ghassemi, Y. S. Kim, et al. *Chem Rev* **2004**, 104, 4587.
212. D. J. Jones and J. Roziere. Chapter In *Handbook of Fuel Cells—Fundamentals, Technology and Applications*, Vol. 3, W. Weslich, A. Lamm, H. A. Gasteiger, eds. John Wiley & Sons, Ltd., New York, 2003; p. 447.
213. A. B. Yaroslavtsev. *Solid State Ionics* **2005**, 176, 2935.
214. N. P. Gnusin, M. V. Pevnitskaya, V. K. Varentsov, et al. USSR patent No 216622. Publ. 21.10.72, 1972.
215. V. I. Zabolotsky, V. V. Nikonenko, N. D. Pismenskaya, et al. Russ. Patent No 2033850, B01 D 13/02, 1995.
216. G. Eigenberger, H. Strathmann, A. Grabovskiy. Germany Patent WO 2005/009596 A1, B01D 61/44, 2005.
217. V. I. Zabolotskii, S. A. Loza, M. V. Sharafan. *Russ J Electrochem* **2005**, 41, 1053.
218. C. Larchet, V. I. Zabolotsky, N. Pismenskaya, et al. *Desalination* **2008**, 222 (1), 489.
219. T. Sata. *J Membr Sci* **2000**, 167, 1.
220. K. Takata, Y. Yamamoto, T. Sata. *J Membr Sci* **2000**, 179, 101.
221. K. Takata, H. Ihara, T. Sata. *Angew Macromol Chem* **2003**, 236, 67.
222. T. Sata and Y. Mizutani. *J Polym Sci* **2003**, 17, 1199.
223. Y. Hu, M. Wang, D. Wang, et al. *J Membr Sci* **2008**, 319, 5.
224. K. Kerose, F. Janowski, V. A. Shaposhnik. *J Membr Sci* **1997**, 127, 17.
225. Z. Amor, S. Malki, M. Taky, et al. *Desalination* **1998**, 120, 263.
226. R. Yamane, Y. Mizutani, H. Motomura, et al. *Denki Kagaku* **1964**, 32, 277.
227. Y. Oren, I. Rubinstein, C. Linder, et al. *Environ Eng Sci* **2002**, 19, 512.
228. V. D. Grebenyuk, R. D. Chebotareva, S. Peters, et al. *Desalination* **1998**, 115, 313.

YU

229. R. K. Nagarale, V. K. Shahi, R. Schubert, et al. *J Colloid Interface Sci* **2004**, 270, 446.
230. V. V. Nikonenko, N. D. Pis'menskaya, E. I. Volodina. *Russ J Electrochem* **2005**, 41, 1205.
231. J.-H. Choi and S.-H. Moon. *J Colloid Interface Sci* **2003**, 265, 93.
232. N. D. Pismenskaya, E. I. Belova, V. V. Nikonenko, et al. *Desalin Water Treat* **2010**, 21, 109.
233. V. G. Levich. *Physicochemical Hydrodynamics*. Prentice-Hall, New York, 1962.
234. H. A. Stone, A. D. Stroock, A. Ajdari. *Annu Rev Fluid Mech* **2004**, 36, 381.
235. N. Churaev, V. Sobolev, A. Somov. *J Colloid Interface Sci* **1984**, 97, 574.
236. C.-H. Choi, K. J. A. Westin, K. S. Breuer. *Phys Fluids* **2003**, 15 (10), 2897.
237. M. Majumder, N. Chopra, R. Andrews, et al. *Nature* **2005**, 438, 44.
238. O. I. Vinogradova and G. E. Yakubov. *Langmuir* **2003**, 19, 1227.
239. O. I. Vinogradova, N. F. Bunkin, N. V. Churaev, et al. *J Colloid Interface Sci* **1995**, 173, 443.
240. V. V. Nikonenko, N. D. Pismenskaya, E. I. Belova, et al. Proceedings of XVIII Mendeleev Congress on General and Applied Chemistry. Moscow, 2007.
241. M. V. Sharafan, V. I. Zabolotskii, V. V. Bugakov. *Russ J Electrochem* **2009**, 45 (100), 1162.
242. A. B. Yaroslavtsev. *Russ J Inorg Chem* **2000**, 45, 249.
243. B. Bonnet, D. J. Jones, J. Roziere, et al. *J New Mater Electrochem Syst* **2000**, 3, 87.
244. G. Kickelbick. *Prog Polym Sci* **2003**, 28, 83.
245. G. Alberti, U. Costantino, J. Kornyei, et al. *Reactive Polym* **1985**, 4, 1.
246. M. Casciola, U. Costantino, A. Peraio, et al. *Solid State Ionics* **1995**, 77, 229.
247. G. Alberti and M. Casciola. *Solid State Ionics* **1997**, 97, 177.
248. E. W. Stein, A. Clearfield, M. A. Subramanian. *Solid State Ionics* **1996**, 83, 113.
249. C. Y. Ortiz-Avila, C. Bharwaj, A. Clearfield. *Inorg Chem* **1994**, 33, 2499.
250. E. Y. Voropaeva, I. A. Stenina, A. B. Yaroslavtsev. *Russ J Inorg Chem* **2008**, 53, 1531.
251. S. A. Novikova, E. I. Volodina, N. D. Pis'menskaya, et al. *Russ J Electrochem* **2005**, 41, 1070.
252. A. S. Shalimov, S. A. Novikova, I. A. Stenina, et al. *Russ J Inorg Chem* **2006**, 51, 700.
253. V. A. Gerasin, T. A. Zubova, F. N. Bahov, et al. *Nanotechnol Russ* **2007**, 2, 90.
254. B. S. Bokshtein and A. B. Yaroslavtsev. *Diffusion of Atoms and Ions in Solids* [in Russian]. MISIS ed. MISIS, Moscow, 2005.
255. E. Y. Voropaeva, I. A. Stenina, A. B. Yaroslatsev. *Russ J Inorg Chem* **2008**, 53, 1677.
256. A. S. Shalimov, A. I. Perepelkina, I. A. Stenina, et al. *Russ J Inorg Chem* **2009**, 54, 356.
257. H. Tang, Z. Wan, M. Pan, et al. *Electrochem Commun* **2007**, 9, 2003.
258. I. A. Stenina, A. A. Lisova, I. Y. Pinus, et al. *Russ Chem Bull* **2008**, 57 (11), 2261.
259. N. P. Berezina, N. A. Kononenko, A. A.-R. Sytcheva, et al. *Electrochim Acta* **2009**, 54 (8), 2342.

260. N. P. Berezina, A. A.-R. Kubaisy, S. V. Timofeev, et al. *J Solid State Electrochem* **2006**, 11, 378.
261. M. Hibino, H. Itoh, K. Kinosita. *J Biophys* **1993**, 64, 1789.
262. N. P. Gnusin, N. P. Berezina, N. A. Kononenko. *Sov Electrochem* **1987**, 23, 127.
263. M. Winter and R. J. Brodd. *Chem Rev* **2004**, 104, 4245.
264. A. M. Bernardes, D. C. R. Espinosa, J. A. S. Tenório. *J Power Sources* **2004**, 130, 291.
265. O. V. Bushkova, I. P. Koryakova, B. I. Lirova, et al. *Dokl Akad Nauk* **2006**, 407, 634.
266. A. L. Rusanov, D. Y. Lihatchev, K. Myullen. *Russ Chem Rev* **2002**, 71 (9), 862.
267. Y. A. Dobrovolsky, P. Jannasch, B. Lafitte, et al. *Russ J Electrochem* **2007**, 43, 489.
268. Y. A. Dobrovolsky, A. V. Pisareva, L. S. Leonova, et al. *Int Sci J Altern Energy Ecol* **2004**, 12, 36.
269. V. V. Starkov, Y. A. Dobrovolsky, N. V. Liskov, et al. *Int Sci J Altern Energy Ecol* **2007**, 6, 24.
270. C. C. Liang. *J Electrochem Soc* **1973**, 120, 1289.
271. J. Maier. *Prog Solid State Chem* **1995**, 23, 171.
272. A. B. Yaroslavtsev. *Russ Chem Rev* **2009**, 78 (11), 1013.
273. R. Jiang, H. R. Kunz, J. M. Fenton. *J Membr Sci* **2006**, 272, 116.
274. G. Alberti, M. Casciola, D. Capitani, et al. *Electrochim Acta* **2007**, 52, 8125.
275. S. A. Novikova, G. Y. Yurkov, A. B. Yaroslavtsev. *Mendeleev Commun* **2010**, 20, 89.
276. E. Y. Voropaeva, E. A. Sanginov, V. I. Volkov, et al. *Russ J Inorg Chem* **2008**, 53, 1536.
277. S. A. Novikova, E. Y. Safronova, A. A. Lysova, et al. *Mendeleev Commun* **2010**, 20, 156.
278. E. Y. Safronova, I. A. Stenina, A. B. Yaroslavtsev. *Russ J Inorg Chem* **2010**, 55, 13.
279. A. B. Yaroslavtsev. *Russ J Inorg Chem* **2010**, 55, 13.
280. R. H. Garrett and C. M. Grisham. *Biochemistry*. Brooks-Cole, Belmont, CA, 2005.
281. N. Pismenskaia, P. Sistat, P. Huguet, et al. *J Membr Sci* **2004**, 228 (1), 65.

YU